JPET Fast Forward. Published on February 26, 2015 as DOI: 10.1124/jpet.114.220335
This article has not been copyedited and formatted. The final version may differ from this version.

A small molecule with anticancer and antimetastatic activities induces rapid mitochondrial-associated necrosis in breast cancer

Anja Bastian, Jessica E. Thorpe, Bryan C. Disch, Lora C. Bailey-Downs, Aleem Gangjee, Ravi K. V. Devambatla, Jim Henthorn, Kenneth M. Humphries, Shraddha S. Vadvalkar, Michael A. Ihnat

Department of Pharmaceutical Sciences (AB, JET, BCD, MAI), Department of Physiology (AB), Flow Cytometry and Imaging Laboratory (JH) at the University of Oklahoma Health Sciences Center, Oklahoma City, OK

DormaTarg, Inc., Oklahoma City, OK (BCD, LCBD, MAI)

Division of Medicinal Chemistry, Graduate School of Pharmaceutical Sciences, Duquesne University, Pittsburgh, PA (AG, RKD)

Oklahoma Medical Research Foundation, Oklahoma City, OK (KMH, SSV)

Running Title: AG311 induces necrosis in breast cancer

Corresponding Author:

Michael A. Ihnat, PhD

Department of Pharmaceutical Sciences

OU College of Pharmacy

PO Box 26901

Oklahoma City, OK 73126-0901

Phone: 271-6593 ext. 47965

Email: michael-ihnat@ouhsc.edu

Number of text pages (excluding references and figure legends): 29

Number of tables: 0

Number of figures: 9

Number of references: 58

Number of words in Abstract: 213

Number of words in Introduction: 473

Number of words in Discussion: 1190

Supplemental section: Total 5 pages with 5 figures and three 3 videos

Nonstandard abbreviations:

AG311, 5-[(4-Methylphenyl)thio]-9H-pyrimido[4,5-b]indole-2,4-diamine; DMSO, dimethyl sulfoxide; DAPI, 4',6-diamidino-2-phenylindole; PARP, poly (ADP-ribose) polymerase; TMRM, tetramethylrhodamine methyl ester; HRP, horseradish peroxidase; ANOVA, analysis of variance; GFP, green fluorescent protein; HUVEC, human umbilical vein endothelial cells; TKI, tyrosine kinase inhibitors; TNBC, triple-negative breast cancer;

BLBC, basal-like breast cancer; EGFR, epidermal growth factor receptor; ER, estrogen receptor; PR, progesterone receptor; Her2/NEU, human epidermal growth factor receptor 2; STS, staurosporine; H&E, hematoxylin and eosin; PI, propidium iodide, HMGB1, high-mobility group protein B1; IC_{50}, half maximal inhibitory concentration; i.p., intraperitoneal; NOAEL, no observed adverse effect level; MTD, maximal tolerated dose; LA, lipoic acid; CsA, cyclosporine A; ΔΨm, mitochondria membrane potential; MW, molecular weight

Recommended Section:

Drug Discovery and Translational Medicine

ABSTRACT

Therapy for treatment-resistant breast cancer provides limited options and the response rates are low. Therefore, the development of therapies with alternative chemotherapeutic strategies is necessary. 5-[(4-Methylphenyl)thio]-9H-pyrimido[4,5-b]indole-2,4-diamine (AG311), a small molecule, is being investigated in preclinical and mechanistic studies for treatment of resistant breast cancer through necrosis, an alternative cell death mechanism. *In vitro*, AG311 induces rapid necrosis in numerous cancer cell lines as evidenced by loss of membrane integrity, ATP depletion, HMGB1 translocation, nuclear swelling, and stable membrane blebbing in breast cancer cells. Within minutes, exposure to AG311 also results in mitochondrial depolarization, superoxide production and increased intracellular calcium levels. Additionally, upregulation of mitochondrial oxidative phosphorylation results in sensitization to AG311. This AG311-induced cell death can be partially prevented by treatment with the mitochondrial calcium uniporter inhibitor, Ru360, or an antioxidant, lipoic acid. Additionally, AG311 does not increase apoptotic markers such as cleavage of poly (ADP-ribose) polymerase (PARP) or caspase 3 and 7 activity. Importantly, *in vivo* studies in two orthotopic breast cancer mouse models (xenograft and allograft) demonstrate that AG311 retards tumor growth and reduces lung metastases better than clinically used agents; and has no gross or histopathological toxicity. Together, these data suggest that AG311 is a first-in-class antitumor and antimetastatic agent inducing necrosis in breast cancer tumors, likely through the mitochondria.

INTRODUCTION

Cancer is a highly heterogeneous disorder that requires an arsenal of treatments - surgery, radiation, and drugs acting through different mechanisms - to affect a successful therapeutic outcome. In spite of over 100 new anticancer agents having been added over the past 20 years in the United States, overall survival rates have only improved in a few cancers and largely because of earlier and better detection (American Cancer Society, 2011). The newer “targeted” agents such as receptor tyrosine kinase inhibitors (TKIs) have fewer side effects than traditional cytotoxic agents, but still have several limitations. Many of these agents are cytostatic, their effect is reversible and importantly, resistance builds rapidly in the form of mutations in the drug target or downstream signaling molecules (Ohashi *et al.*, 2013). It is estimated that 80% of tumors become resistant to drug therapy (Clarke *et al.*, 2001). Development of resistance to apoptosis during cancer progression is a hallmark of cancer (Hanahan and Weinberg, 2011). Since apoptosis is the primary death pathway of many chemotherapeutic agents, alternative cell death mechanisms such as necrosis can prove beneficial to circumvent chemoresistance (Olofsson *et al.*, 2007; de Bruin and Medema, 2008). Current examples of approved anti-cancer therapies that induce necrosis include photodynamic therapy and alkylating agents (Zong *et al.*, 2004; Yoo and Ha, 2012). In addition, other agents triggering necrosis are being preclinically evaluated for anti-cancer activity, for example β-lapachone, apoptolidin, and honokiol (Ricci and Zong, 2006). The role of mitochondria in apoptotic cell death is well characterized, but more recently a new link between mitochondrial dysfunction and necrosis has been established (Hamahata *et al.*, 2005; Choi *et al.*, 2009; Kinnally *et al.*, 2011). Features of drug-induced mitochondrial dysfunction include the opening of the membrane permeability transition pore and oxidative stress. Mitochondrial inhibitors such as metformin have shown clinical anticancer efficacy in preclinical animal models and diabetic patients. (Whitaker-

Menezes *et al.*, 2011).

In this work, we begin to characterize the cell death mechanisms and describe the anti-tumor and antimetastatic activity of a small molecule, AG311, in treatment-resistant breast cancer. TNBC (triple-negative breast cancer) and BLBC (basal-like breast cancer) are resistant to chemotherapy, inherently aggressive, metastatic, and have a poor prognosis. TNBC lacks EGFR-2 (Her2/NEU), a key target for TKI therapy, and hormone receptors (estrogen receptor and progesterone), targets for anti-hormone therapy. TNBC/BLBC also metastasize to lung, brain, and bone and like most tumors, once metastasized, are refractory to treatment (Yuan *et al.*, 2014). We report that TNBC/BLBC cells are sensitive to AG311 in culture and *in vivo* while noncancerous cells are relatively resistant. Further, unlike most other small molecules, AG311 induces rapid membrane permeabilization and mitochondrial dysfunction and shows multiple characteristics of necrotic cancer cell death in culture. Most importantly, AG311 is more efficacious *in vivo* than current therapies in a BLBC orthotopic xenograft and a TNBC orthotopic allograft lung metastasis model.

MATERIALS AND METHODS

Cell culture

Cancer cell lines were purchased from American Type Culture Collection (Manassas, VA), except MDA-MB-435, which was a kind gift of Dr. Janet Price at MD Anderson Cancer Center in the mid-1990s and shown to be free of M14 melanoma cross-contamination (Chambers, 2009). All cells, with the exception of HUVEC, were maintained in Dulbecco's Modified Eagles Medium (DMEM) (Thermo Fisher Scientific, Waltham, MA) with 10% Cosmic Calf Serum (CCS) (HyClone, Logan, UT) and added glutamine/pyruvate (HyClone) at 37°C with 5% CO_2. HUVECs were cultured in Media-199 with 10% CCS and added glutamine/pyruvate. For galactose studies, cells were cultured for five days in glucose-free DMEM (Life Technologies, Carlsbad, CA) supplemented with 10 mM galactose or 25 mM glucose before treatment. For spheroids, MDA-MB-435 cells were plated at 15,000 cells/well on 1% agarose. Cells formed clusters overnight and were cultured for 12 days to form spheroids with one-half of the media replaced daily.

Compound

AG311 was designed and synthesized by A. Gangjee et al (Gangjee *et al.*, 2010).

Viability assay

Cells were seeded in 96-well plates (#3904 Corning, New York, NY) at 5 x 10^3 cells/well and allowed to attach overnight. MDA-MB-435 cells were pretreated with 5 µM or 7.5 µM BAPTA-AM (EMD Milllipore, Billerica, MA), 1, 7.5, or 15 µM Ru360 (EMD Milllipore), 200 µM lipoic acid (LA) (Sigma-Aldrich, St. Louis, MO), or 1 µM cyclosporine A (CsA) (Enzo Life Sciences, Farmingdale, NY) in Opti-MEM (Life Technologies) for 30 minutes before

JPET Fast Forward. Published on February 26, 2015 as DOI: 10.1124/jpet.114.220335
This article has not been copyedited and formatted. The final version may differ from this version.

addition of AG311 (50 mM DMSO stock diluted in Opti-MEM). After 4 hours of treatment with AG311, 10% serum was added and cells incubated for an additional 44 hours unless otherwise indicated. To assess viability, PrestoBlue (Life Technologies) was added as per manufacturer's protocol and read on a microplate reader (BioTek, Winooski, VT). IC_{50} values were determined by nonlinear regression analysis in Prism 6.0 software (GraphPad, San Diego, CA).

Membrane permeability

SYTOX Green (Life Technologies) (0.5 µM in Opti-MEM) was added to MBA-MD-435 cells (5 x 10^3/well) 10 minutes prior to drug treatment or pretreatment with Ru360 (30 min). Dye uptake was measured on a microplate reader (485/530nm) every 15 minutes for 3 hours. For the 24-hour membrane permeability time course, cells were incubated with SYTOX Green (Life Technologies) and Hoechst 33342 (Life Technologies) for 10 minutes before addition of AG311. Images were acquired throughout at different intervals using Operetta High Content Imaging System (Perkin Elmer, Waltham, MA). Uptake of SYTOX (green) represents all the permeabilized cells and Hoechst 33342 (blue) stained cells represent the total number of cells (live and dead) in the field. The percentage of green to blue stained cells was graphed. Cells were also treated with AG311 in HBSS with or without calcium in the presence of SYTOX Green and imaged every minute by JuLi Smart Fluorescent Imager (BulldogBio, Portsmouth, NH) (25x, 466/535nm).

The effect of AG311 on MDA-MB-435 cells and HDF cells in a mixed culture system. The MDA-MB-435 and HDF cells were incubated with Cell Tracker Red (1 µM) or Cell Tracker Green (2 µM) (Life Technologies), respectively, for 30 min in serum-free media at 37ºC. Cells were washed once in PBS and cultured at equal ratio of 3000 red MDA-

MB-435 and 3000 green HDF cells overnight. The media was replaced with SYTOX blue (Life Technologies) diluted in Opti-MEM and cells treated with AG311. Images were acquired every 5 min with 10x objective using Operetta High Content Imaging System (Perkin Elmer).

Cellular ATP content measurement

Cells were treated with AG311 and ATP levels were measured using ATP Detection Assay Kit (ab113849, Abcam, Cambridge, MA) according to manufacturer's instructions The data was normalized to ATP content of untreated cells.

Lactate dehydrogenase release

Lactate dehydrogenase release (LDH) release from cells after drug treatment was measured with LDH Cytotoxicity Assay Kit (Cayman Chemical, Ann Arbor, MI) per manufacturer's protocol.

Apoptosis assessment

MDA-MB-435 cells were treated with AG311 or 1 μM staurosporine (STS) (Enzo Life Sciences). Immunoblotting was performed as described (Kamat *et al.*, 2007) using the following antibodies: cleaved PARP (#9541, Cell Signaling, Danvers, MA) or β-actin (#4970, Cell Signaling, 1:1000) and anti-rabbit HRP (#7074, Cell Signaling, 1:2000). Membranes were imaged using FluorChem-HD2 imaging system (ProteinSimple, Santa Clara, CA). AG311-induced caspase 3 and 7 activities were measured with caspase-Glo 3/7 assay kit (Promega, Madison, WI) per manufacturer's instructions, and luminescence read with a BioTek microplate reader.

Live cell imaging

SYTOX Green (Life Technologies), $DiBAC_4(3)$ (Life Technologies), tetramethylrhodamine methyl ester (TMRM) (Biotium, Hayward, CA), MitoSOX (Life Technologies), MitoTracker Green (Life Technologies) (DMSO) were diluted to 1 µM, 5 µM, 10 nM, 2.5 µM, and 200 nM in Opti-MEM, respectively. Propidium iodide (PI) (Sigma) (in water) was diluted to 7.5 µM in Opti-MEM. Cells were incubated with SYTOX Green, MitoSOX, PI for 15 minutes; TMRM and $DiBAC_4(3)$ for 30 minutes; or MitoTracker Green for 45 minutes. MitoSOX and MitoTracker Green dyes were replaced with Opti-MEM after incubation. Color and brightfield images were acquired simultaneously every minute using a Nikon TE2000-E inverted epifluorescence microscope (20x or 40x) equipped with a temperature control and CO_2 chamber (37°C/5% CO_2). Images were processed with MetaMorph software (Sunnyvale, CA).

Intracellular calcium

MDA-MB-435 cells (180,000 cells per well of 6-well plate) were loaded with Fluo-4 Direct (Life Technologies) and 2.5 mM probenecid (Life Technologies) added to improve cellular retention. Cells were treated with AG311 in the presence of 7.5 µM PI with images acquired every minute at 40x (490/555nm).

HMGB1 translocation

MDA-MB-435 ($2.8x10^4$) cells were treated with AG311 and immunostained with anti-HMGB1 (1:100) (#3935, Cell Signaling) and anti-rabbit Alexa-Fluor-488 (1:500) (Life Technologies) as previously described (Dandajena *et al.*, 2012). Additionally, immunoblotting was performed for HMGB1 as described above for cleaved PARP. For this, MDA-MB-435 cells were treated with AG311 (25 µM) for 30 and 60 min or solvent control. The cytosolic cell lysates were collected with Nuclear Extraction kit (Affymetrix Panomics, Santa Clara, CA) as per manufacture's protocol. Immunoblots were

incubated with HMGB1 (1:1000) overnight. Levels of vinculin (Sigma) (1:4000) were used as the loading control. Densitometry was performed for both HMGB1 and vinculin using Image Lab software V5.2.1 (BioRad , Hercules, CA). The values are represented as the ratio of HMGB1 to vinculin levels.

Mitochondrial membrane potential

MDA-MB-435 cells (suspension or $5x10^4$ per well of 96-well plate) were incubated (30 min) with TMRM (10 nM) in Opti-MEM and fluorescence readings acquired continuously for 20 minutes using FL-2 filter (EX 585/20nm) with Accuri C6 (BD Biosciences). After 5 minutes, AG311 or solvent control was added to the cell suspension. Fluorescence intensities were also measured using a microplate reader. Additionally, cells were treated with AG311 for different durations (0 – 240 min) or treated with solvent control (0.2% DMSO). Cells were then incubated in suspension with JC-1 (Cayman, Ann Arbor, MI; 5 µM) in Opti-MEM for 30 min, washed twice, and immediately measured with FACS Calibur (BD Biosciences) at 488 and 633nm.

Superoxide measurement

MDA-MB-435 cells (5×10^3 cells per well of 96-well plate) were loaded with MitoSOX 2.5 µM in Opti-MEM for 15 min and solution replaced with AG311 or solvent control (0.2% DMSO) in Opti-MEM and fluorescence intensities were measured with a BioTek plate reader (EX530 nm/EM590 nm).

Cell exclusion zone assay

4T1-luc2-GFP cells (1.5×10^4 per well of 96-well plate) were seeded around the barrier of Oris Cell Migration Assay 96-well plate (Platypus, West Lebanon, NH). Cells were grown overnight followed by removal of the circular barrier and treatment with AG311,

JPET Fast Forward. Published on February 26, 2015 as DOI: 10.1124/jpet.114.220335
This article has not been copyedited and formatted. The final version may differ from this version.

latrunculin A (Cayman), or solvent control (0.2% DMSO) for 32 hours. At the end of the experiment, Calcein-AM (Life Technologies) (2 µM) was added and wells imaged using Operetta High Content Imaging System (Perkin Elmer) with 2x objective and (EX500 nm/EM540 nm). The area was measured with Columbus Software 2.4.2 (Perkin Elmer) and normalized to solvent treated control. To distinguish cell migration from proliferation, cell growth was arrested with mitomycin C (Enzo Life Sciences) (10 µM for 2 hours) prior to drug treatment. Viability of treated cells was determined with PrestoBlue at the end of the experiments. No signs of toxicity in cells were observed for treatment with mitomycin C and/or AG311. This experiment required a higher cell seeding density then other cell assay, thus resulting in higher IC_{50} values.

Mouse dose-finding

For *in vivo* drug administration, the no observed adverse effect level (NOAEL) and the maximal tolerated dose (MTD) were determined using NCr nu/nu athymic mice (Charles River, Wilmington, MA) and BALB/cJ mice (Jackson Laboratories, Bar Harbor, ME). Compounds were prepared as mg/ml solution dissolved in 1**:**1.8**:**7.2 ratio DMSO/ solutol-15 (BASF, Ludwigshafen, Germany)/D5W (5% dextrose in water). Starting doses were 10 and 15 mg/kg (n = 2 mice per treatment) and every two days mice were weighed and doses increased in 10 mg/kg increments if no weight loss was observed. Upon weight loss, the experiment was stopped and the current dose used as an estimated MTD. The dose before observed weight loss was estimated to be the NOAEL.

4T1 triple negative orthotopic allograft

To determine the effect of AG311 on necrosis *in vivo,* BALB/cJ mice were implanted with non-fluorescent 4T1 tumor cells. The experiment was performed as published (Bailey-Downs et al., 2014) with the following modifications: Cell suspension (7500 cells/ 100µL)

in PBS with 1 mM EDTA was implanted into the mammary fat pad #4 of 8 week old female BALB/cJ mice. Three weeks after implantation when the average tumor size was ~260 mm^3, mice were separated based on matched tumor volumes (n = 9-11). AG311 (23 mM stock) or solvent control (1:1:8 DMSO:solutol:saline) was injected intratumorally once daily for two days with treatment volumes adjusted to 1/15 of tumor volume. Twenty-four hours post treatment, mice were euthanized, tumors excised, cut into two equal parts, fixed overnight, paraffin embedded and hematoxylin and eosin (H&E) stained (Precision Histology, Oklahoma City, OK). To assess tumor necrosis, two tumor sections throughout the tumor were imaged by light microscopy (0.5x). The percentage of necrosis per total area was determined using ImageJ 1.48v software by a blinded investigator. Due to the large necrotic regions in the drug-treated tumors, parts of tumor sections became dissociated prior to processing. For area determination, the lines were drawn straight across this gap for all tumor sections. Necrotic areas were confirmed by a veterinary pathologist. In a separate experiment, to determine drug efficacy, BALB/cJ mice were implanted with 4T1-luc2-GFP cells as described above. Five days after implantation, mice were intraperitoneally injected with AG311 (50 mg/kg) twice weekly for a total of five doses, docetaxel (15 mg/kg) once weekly, or solvent control (1:1.8:7.2 DMSO:solutol:saline) twice weekly**.** Tumor size was determined using Vernier calipers and tumor volume calculated (0.52*(length*width*depth)). Weights were determined twice weekly. Lungs were removed, imaged using JuLi Imager (Bulldog Bio) at 25x and number of metastases per lung counted.

MDA-MB-435 orthotopic xenograft

The detailed methods for this model have been described elsewhere (Ihnat *et al.*, 1999). Briefly, human MDA-MB-435 GFP-tagged cells (500,000) in DMEM were implanted into the mammary fat pad of 7 week old female NCr nu/nu athymic mice. Five days post-

implantation, the presence of tumors was determined using fluorescence animal imaging system (LT-9MACIMSYSPLUSC, LightTools, Tokyo). Animals were treated intraperitoneally (i.p.) twice weekly for 30 days with AG311 (45 mg/kg) or once weekly with doxorubicin (1 mg/kg) or carrier control**.** Tumor size was determined using Vernier calipers and tumor volume calculated (0.52*(length*width*depth)). At experimental end, animals were humanely euthanized with CO_2 asphyxiation (AALAC approved), lungs removed, imaged (LightTools), and metastases counted with Spot Basic software (Sterling Heights, MI).

Rat toxicity study

Sprague-Dawley rats (3 male, 3 female; 9 weeks of age) were treated i.p. with 22.5 mg/kg AG311 twice weekly for 4 weeks. This dose was chosen on the basis that rats have twice the weight/surface area ratio as compared to mice; consequently the MTD of 45 mg/kg in mice converts to 22.5 mg/kg in rats (Reagan-Shaw *et al.*, 2008). At 28 days, gross pathological analysis of fur, skin, appendages, stomach, colon, spleen, heart, liver, kidneys and lungs, and histopathological analyses of H&E slides of heart, liver, kidneys, and lungs were performed by a veterinary pathologist. For this, the organs were fixed embedded, sectioned, and H&E stained.

Statistical analysis

All data are expressed as mean ± S.E.M from at least 3 experiments unless otherwise stated. *P*-values were calculated using two-tailed unpaired Student's t test or One-way ANOVA with an appropriate post-test unless otherwise stated. $P < 0.05$ was considered statistically significant. *$P < 0.05$, **$P < 0.01$, ***$P < 0.001$, versus solvent (0.2% DMSO); †$P < 0.05$, ††$P < 0.01$, †††$P< 0.001$ versus docetaxel or doxorubicin treatment or HDF.

JPET Fast Forward. Published on February 26, 2015 as DOI: 10.1124/jpet.114.220335
This article has not been copyedited and formatted. The final version may differ from this version.

RESULTS

Cytotoxicity of AG311 in cancer and normal cells

The cytotoxicity IC_{50} values of AG311 (Structure: **Fig. 1A**), ranging from 5.9 to 29.3 μM, were determined by a microplate viability assay from fifteen cancer cell lines (**Fig. 1B**)**.** The IC_{50} value for MDA-MB-435 (BLBC) was 13.9 μM. In other breast cancer cell lines, AG311 had similar (MDA-MB-468 and MCF-7) or lower (MDA-MB-231) IC_{50} values compared to MDA-MB-435. AG311 was least potent on noncancerous human dermal fibroblasts HDF (IC_{50} 29.3 μM), suggesting a level of selectivity. **Figure 1C** shows the dose response curves of AG311 on three different TNBC/BLBC cell lines and HDF cells. AG311 has a steep dose response curves (**Fig. 1B**), unlike other traditional anticancer compounds (**Supplemental Figure 1**).

AG311 induces membrane permeabilization

SYTOX is a membrane impermeable intercalating dye that increases in fluorescence intensity when the cell membrane is compromised. AG311-treatment results in a rapid increase in fluorescence intensity within 30 minutes (25 μM) or 60 minutes (20 μM) (**Fig. 1E, 1F**), indicating that AG311 is rapidly permeabilizing the membrane to molecules of <~600 Da, the MW of SYTOX. Additionally, a time-course of AG311 exposure in MDA-MB-435 cells results in the formation of large, stable, and continuously expanding membrane blebs simultaneous to SYTOX uptake (**Fig. 1D**) (video in supplemental). The formation of these blebs is indicative of necrosis in contrast to transient blebbing observed in apoptosis (Barros *et al.*, 2003). The occurrence of membrane hyperpermeability (**Fig. 1E**) correlates temporally with decreased cell viability determined by the resazurin dye PrestoBlue (**Fig. 1H**). Increasing AG311 concentration from 20 to 40μM resulted in both a rapid (15-60 min) increase in membrane hyperpermeability (**Fig. 1E**) and a decrease in cell viability (**Fig. 1H**). In contrast, 10 μM

JPET Fast Forward. Published on February 26, 2015 as DOI: 10.1124/jpet.114.220335
This article has not been copyedited and formatted. The final version may differ from this version.

AG311, a dose slightly above the IC_{50} value, did not result in a decrease in viability or an increase in membrane permeability until 6 hours after treatment. From 6 hours onward a decrease in viability and increase in membrane permeability was observed. (**Fig. 1E and H**). This data illustrates that for all tested doses, the effect of AG311 on membrane permeability and viability is not transient. A cell culture model that more closely resembles the three dimensional structure of tumors are multicellular spheroids. MDA-MB-435 spheroid cultures were exposed to AG311 in the presence of SYTOX Green and similar to monolayer cells, membrane hyperpermeability was observed in spheroids after 30 minutes (**Supplemental Figure 2)**.

AG311 selectively induces membrane permeabilization

AG311 was less effective in inducing membrane hyperpermeability in normal HUVEC (noncancerous cells) versus tumor cells (**Fig. 1F**). AG311-treated HUVEC cells (25 µM) displayed delayed membrane hyperpermeability compared to MDA-MB-435 cells (**Fig. 1F**)**,** but more notably, 20 µM AG311 did not result in membrane hyperpermeability after 6 hours, whereas this occurred rapidly in MDA-MB-435 cells (**Fig. 1F**). This correlates with the differential IC_{50} values in cancerous (MDA-MB-435) versus noncancerous (HDF) cells (**Fig. 1B**). To further show selectivity, mixed cell culture of human dermal fibroblasts (HDF) and breast cancer cells (MDA-MB-435) labeled green or red, respectively, were treated with AG311. Only MDA-MB-435 cells underwent cell death after treatment with AG311 during the studied duration (90 min) as shown by uptake of SYTOX Blue **(Fig 1G)** (video in supplemental data). This demonstrates that AG311 selectively induces cell death in breast cancer cells.

AG311 induces necrosis and lacks molecular markers of apoptosis

To further investigate AG311-induced membrane compromise, release of lactate

dehydrogenase, a 36 kDa protein commonly used to detect necrosis-associated membrane changes was measured (Chan *et al.*, 2013). After AG311-treatment, LDH levels increased significantly (**Fig. 2A**). Additionally, the cellular localization of the high mobility group B1 (HMGB1) protein was determined (Scaffidi *et al.*, 2002). In untreated cells, HMGB1 is sequestered in the nucleus but upon induction of necrosis it is released into the cytoplasm, where it acts as an inflammatory stimulator (Scaffidi *et al.*, 2002). Treatment with AG311 (25 μM) resulted in translocation of HMGB1 to the cytoplasm after 20 min as shown by immunocytochemistry (**Fig. 2D**) and immunoblotting (30 and 60 min). (**Fig 2E**). Another hallmark of necrosis is nuclear swelling. The nuclear diameter of AG311-treated MDA-MB-435 cells was also significantly greater compared to untreated controls, indicating necrosis (**Fig. 2B**). In contrast to apoptosis, which is an ATP dependent process (Golstein and Kroemer, 2007), necrosis is energy-independent and results in rapid ATP depletion. MDA-MB-435 cells exposed to AG311 resulted in significant decreases in ATP levels after 15 min and complete ATP depletion by 180 min (**Fig. 2C**). Together with the findings of membrane swelling, stable blebbing and rapid membrane hyperpermeabilization, these data suggest that AG311 rapidly induces necrosis. To further exclude the possibility of apoptotic cell death, the induction of apoptotic markers was investigated. Exposing cells to AG311 did not induce PARP cleavage (**Supplemental Figure 3A**) or increase caspase-3/7 activity (**Supplemental Figure 3B**), further suggesting that AG311 does not induce apoptosis.

AG311 affects calcium homeostasis

Increased intracellular calcium is another characteristic of necrotic cell death and can lead to mitochondrial disruption (Golstein and Kroemer, 2007). To investigate this, the calcium-specific fluorescent indicator Fluo-4 was used. Exposure of MDA-MB-435 cells to AG311 resulted in an increase in intracellular calcium levels (Fluo-4 fluorescence

intensity) within 40 minutes. Membrane hyperpermeability, indicated by propidium iodine uptake (MW 668), which is comparable to SYTOX, occurred temporally after intracellular calcium increase (**Fig. 3A**) (video in supplemental data). Further, it was determined whether extracellular calcium was required for cell death and membrane hyperpermeability. Cells exposed to AG311 in calcium free media (HBSS) resulted in similar membrane permeability and blebbing after 60 minutes as in calcium-containing media (**Fig. 3B**), indicating that extracellular calcium is not required for AG311-induced cell death. Pretreatment with the calcium chelator, BAPTA-AM, significantly, but only slightly protected against AG311-induced cell death (**Fig 3C**). Together this illustrates that levels of calcium increase, but do not seem to play a major role in the AG311-induced cell death pathway.

AG311 induces plasma membrane depolarization

The fluorescent dye, $DiBAC_4(3)$ is commonly used to assess changes in plasma membrane potential. Depolarization of the membrane increases the electrochemical gradient and draws $DiBAC_4(3)$ into the cell, resulting in increased fluorescence (Epps *et al.*, 1994). Exposure of MDA-MB-435 cells to AG311 (20 and 25 μM) resulted in rapid decreases in fluorescence intensity, indicative of hyperpolarization, followed by increases in fluorescence, indicative of membrane depolarization (**Fig. 3D**). The timing of the depolarization phase correlates closely with the timing for membrane permeability to SYTOX (**Fig. 3D** vs **Fig. 1E**). Lower doses of AG311 (15 μM) did not result in membrane permeability to SYTOX (MW ~600Da), but did result in hyperpolarization within one hour. Together these data indicate that AG311 is perturbing the membrane early in the cell death process leading to alterations in membrane potential.

AG311 induces rapid mitochondrial membrane changes

JPET Fast Forward. Published on February 26, 2015 as DOI: 10.1124/jpet.114.220335
This article has not been copyedited and formatted. The final version may differ from this version.

AG311-induced mitochondrial membrane potential, ΔΨm, fluctuations were assessed by measuring the fluorescence of a mitochondria specific dye, tetramethylrhodamine methyl ester (TMRM), which accumulates in the mitochondria based on the ΔΨm and localizes to the mitochondrial matrix in inverse proportion to the ΔΨm (Perry *et al.*, 2011). Exposure to AG311 resulted in rapid mitochondrial depolarization within five minutes as observed by a decrease in TMRM fluorescence intensity using fluorescence microscopy (**Fig. 4A**) and flow cytometry (**Fig. 4B**). These findings were confirmed by measurement of the cationic dye JC-1, which forms red-fluorescent J-aggregates at normal/high ΔΨm and green-fluorescent monomers upon depolarization of the ΔΨm (Chazotte, 2011). AG311 resulted in a decrease in the ratio of aggregates (red) over monomers (green) in MDA-MB-435 cells at 15 minutes post-treatment (**Fig. 4C**), thus indicating mitochondrial membrane depolarization. The red fluorescent cell population with aggregated JC-1 shifted from quadrant 2 (Q2) to quadrant 1 (Q1) (**Fig. 4C**), indicating ΔΨm depolarization in response to AG311. Additional time points (30 – 240 min) from flow cytometry studies showed a similar shift in fluorescence (**Fig 4D**). This correlates with the results obtained using TMRM, supporting the hypothesis that AG311 induces rapid mitochondrial depolarization.

AG311 induces mitochondrial dysfunction

To further elucidate the effect of AG311 on calcium and mitochondria function, an inhibitor of the mitochondrial calcium uniporter (MCU), Ru360, was used (García-Rivas *et al.*, 2006). Treatment with AG311 in the presence of Ru360 protected against AG311 induced cell death as determined by cell viability after 24 hours (**Fig. 5A**). Pretreatment with Ru360 also protected cells against membrane hyperpermeability induced by AG311 (**Fig. 5B**). To determine whether AG311-induced cell death is mitochondrial dependent, cells were cultured in galactose media. Galactose drives cells to upregulate energy

production through oxidative phosphorylation in the mitochondria, making them more suitable for studying drug-induced mitochondrial dysfunction (Dykens *et al.*, 2008; Aguer *et al.*, 2011). MDA-MB-435 cells cultured in galactose media were significantly more sensitive to AG311-induced cell death, as indicated by reduced viability after 24 hours of drug treatment (**Fig. 5C**), suggesting that for AG311 death is mitochondrial-mediated. Next, it was tested whether the mitochondrial permeability transition pore (MPTP) is involved in AG311-induced cell death by using the specific MPTP inhibitor cyclosporine A (CsA). AG311-induced cell death is independent of MPTP opening, as indicated by failure of the MPTP inhibitor, cyclosporine A (CsA), to protect against AG311-induced cell death (**Supplemental Figure 4**). This suggests that AG311-mediated cell death is dependent upon mitochondrial calcium release that occurs in an MPTP-independent manner.

Role of superoxide in AG311-induced cell death

Necrosis is often associated with oxidative stress (Ryter *et al.*, 2007). The production of mitochondrial superoxide in response to AG311 was determined by MitoSOX using fluorescence microscopy and plate reader analysis. Mitochondrial superoxide production was detectable after only 20 minutes post-treatment (**Fig. 5D**) and maximal superoxide levels were reached before the membrane was permeable to SYTOX (MW ~600 Da) (**Fig. 5D**). Similar to mitochondrial depolarization, low doses of AG311 (15 μM) were able to induce mitochondrial superoxide production (**Fig. 5E**). It was next tested whether a mitochondrial antioxidant, lipoic acid, can protect against AG311 induced cell death (Smith *et al.*, 2004). Pretreatment of cells with lipoic acid followed by treatment with AG311 (7.5 μM, 10 μM, 15 μM) had significantly increased viability as compared to their counterparts not treated with lipoic acid. At higher concentrations of AG311 (20, 30, or 40 μM) lipoic acid did not protect against AG311 (**Fig. 5F**). Collectively this data

JPET Fast Forward. Published on February 26, 2015 as DOI: 10.1124/jpet.114.220335
This article has not been copyedited and formatted. The final version may differ from this version.

indicates that AG311 induces mitochondrial superoxide, which contributes to its induction of cell death.

Inhibition of breast cancer cell migration by AG311

Mitochondrial activity has been shown to be increased in breast cancer metastases (Sotgia *et al.*, 2012; Zhao *et al.*, 2013), and agents such as graphene (Zhou *et al.*, 2014) and metformin (Sanchez-Alvarez *et al.*, 2013) have shown to reduce metastasis via inhibition of the mitochondria. Thus, AG311 could possess antimetastatic activity. The ability to inhibit migration, a hallmark of metastasis, was first evaluated using a cancer cell migration assay. The 4T1-luc2-GFP TNBC cells were used because this cell line is highly metastatic *in vivo* and thus suitable for *in vitro* migration studies. AG311-treatment significantly inhibited cell migration at multiple subtoxic doses in 4T1-luc2-GFP cells (**Fig. 6 A, B**). Treatment with AG311 showed no effect on cell viability at the tested doses (**Fig 6C)**. The IC_{50} values are higher than reported in figure 1A, because in the migration assay, three-fold more cells were plated, shifting the dose-response curve to the right (**Supplemental Figure 5.)** To minimize the influence of cell proliferation on migration, mitomycin C was used to inhibit cell division prior to treatment. With mitomycin C added, AG311 retained the ability to inhibit migration without reducing viability (**Fig. 6 D, E, F).**

AG311 increases necrosis in vivo

In order to assess the ability of AG311 to induce necrosis *in vivo*, AG311 was injected intratumorally into 4T1 orthotopic breast tumors of BALB/cJ mice. *In vivo*, AG311-induced necrosis was quantified by calculating the percentage of necrotic area within the tumor section from H&E stained tumor sections. The AG311-injected tumors had a significantly higher percentage of necrosis as compared to their control treated

JPET Fast Forward. Published on February 26, 2015 as DOI: 10.1124/jpet.114.220335
This article has not been copyedited and formatted. The final version may differ from this version.

counterparts (27.6 mm^2 and 17.5 mm^2, respectively) (**Fig. 7A**). The control treated tumors showed normal necrotic cores attributed to a lack of vasculature within the tumors. Representative images of necrotic areas are shown in **figure 7B**. This demonstrates that AG311 possess the ability to induce necrosis in tumor tissue.

Effect of AG311 on tumor growth, metastases, and toxicity in a MDA-MB-435 orthotopic xenograft model

Next, AG311 was tested for efficacy in a BLBC human breast cancer mouse xenograft model against an agent of choice, anthracycline doxorubicin (Gradishar *et al.*, 2014). First, the no adverse effect level (NOAEL) dose of AG311 (45 mg/kg twice weekly) and the maximal tolerated dose (MTD) for doxorubicin (1 mg/kg twice weekly) was determined in NCr nu/nu athymic mice. Animals were implanted with MDA-MB-435 GFP cells and five days after implantation, treatment was initiated. Treatment with AG311 significantly reduced primary tumor growth as compared to control or doxorubicin (**Fig. 8A**). Additionally, AG311-treated animals had fewer lung metastases at the end of the experiment as compared to control treated animals (**Fig. 8B**) and continued to gain weight throughout the experiment (**Fig. 8C**), indicating low to no systemic toxicity.

Antitumor growth and antimetastatic efficacy and toxicity of AG311 in a TNBC orthotopic allograft model

Next, the efficacy of AG311 was examined in a TNBC allograft metastatic progression model in immune proficient mice, previously developed in our laboratory (Bailey-Downs *et al.*, 2014). Dual luciferase/GFP 4T1-tagged (4T1-luc2-GFP) cells were implanted in female BALB/cJ mice. Animals were treated with NOAEL dose of AG311 (50 mg/kg twice weekly), MTD of docetaxel (15 mg/kg once weekly), or solvent control. AG311 reduced primary tumor growth, as did the agent of choice, docetaxel (**Fig. 8D**), but with

low systemic toxicity as determined by weight change (**Fig. 8F**). More importantly, AG311 significantly reduced the number of lung metastases compared to all groups (**Fig. 8E**).

Toxicity study with AG311

AG311 was tested in rats to determine whether the absence of toxicity in mice holds true for slightly larger mammals. In this study, rats were treated with 22.5 mg/kg AG311, which is equivalent to the MTD of 45 mg/kg in mice. All rats gained weight throughout the study and the mean weight gain was 16.8% for control and 14.8% for AG311-treated rats (no statistical difference). Gross and histopathological evaluation by a veterinary pathologist after four weeks of treatment showed no apparent signs of toxicity in all evaluated organs (liver, kidney, heart, spleen), indicating an absence of systemic toxicity.

DISCUSSION

Cancer is a highly heterogeneous syndrome, both inter- and intratumorally, thus combining an arsenal of effective therapies targeting different pathways is critical to evoke a definitive “cure.” Herein, we describe for the first time a small synthetic molecule, AG311, which possesses *in vivo* robust antitumor and antimetastatic activity in traditionally treatment resistant breast cancers. This agent also appears to act rapidly on the mitochondria resulting in necrotic cell death. Interestingly, this small synthetic molecule displays rapid necrosis similar to a toxin, yet in contrast to toxins, our molecule has no apparent systemic toxicity in animals.

Figure 9 shows a temporal overview of the morphological and molecular changes induced by AG311 in cancer cells. The earliest molecular change observed in response to AG311 is mitochondrial membrane depolarization followed by rapid ATP

depletion. In parallel, early membrane perturbations are observed as hyperpolarization, followed by depolarization once the plasma membrane has become hyperpermeable to small molecules (e.g. SYTOX) and has formed large membrane blebs. Shortly before membrane permeability occurs, intracellular calcium and superoxide levels increase. The latest event observed is complete loss of membrane integrity, at which point the membrane is permeable to proteins (e.g. LDH) and cells considered nonviable.

We showed that AG311 induces rapid mitochondrial depolarization and superoxide production, AG311 is more effective in glucose-free conditions, and that Ru360 inhibited AG311-induced cell death. These findings suggest a key functional role of mitochondria in AG311 cell death. The mitochondria play a central role in cell survival and death and mitochondria-targeted chemotherapy appears promising for the treatment of apoptosis-resistant cancer cells (Costantini *et al.*, 2000; YC Li *et al.*, 2004). A common view is that cancer cells have dysfunctional mitochondria and have increased glycolysis (i.e., Warburg effect). In recent years, this view has been challenged by Lisanti (Witkiewicz *et al.*, 2012) and others (Valencia *et al.*, 2014). Evidence suggests that cancer cells produce energy through oxidative phosphorylation while the surrounding stromal cells are highly glycolytic and fuel the tumor oxidative metabolism. This observation has been termed the “reverse-Warburg” effect and is not only seen in primary tumors, but also in metastases (Bonuccelli *et al.*, 2010). Thus the observed antitumor and antimetastatic effect of AG311 could be mediated through the inhibition of oxidative phosphorylation and limiting the energy production of the tumor cells. The cell data support selectivity of AG311 for cancer cells at low drug concentration (<14 μM), though at higher drug concentrations (30 μM) normal cells also undergo cell death, this selectivity could be a result of the higher energy demand of tumor cells. When energy demand is greater than supply as is seen with necrosis, cells encounter a bioenergetic catastrophe that leads to necrotic cell death (Edinger and Thompson, 2004). Recently, a

mitochondria-directed therapy, VLX600, was described to selectively affect mitochondria in metabolically compromised environments resulting in autophagy (Zhang *et al.*, 2014). Other agents such as honokiol, betulinic acid, and lonidaminde, have also been proposed to cause cancer cell death through opening of the mitochondrial permeability transition pore (Lena *et al.*, 2009). Mitochondrial free radical production by AG311 appears to be part of its cell death mechanism, as antioxidant co-administration decreasing the potency of AG311 demonstrated. Further, perhaps adding an agent like the pyruvate dehydrogenase kinase inhibitor, dichloroacetate, to increase cancer cells' reliance on mitochondrial function may enhance the activity of AG311, similar to the galactose results in cultured cells.

We show that AG311 rapidly induces necrosis. Necrosis was once considered undesirable because it was deemed an unplanned and unregulated form of death. Recently, necrosis was reported to be highly regulated, occurring in a number of physiological and pathophysiological situations (Vanden Berghe *et al.*, 2014). It was further thought that necrosis was inherently undesirable in terms of cancer therapy because it resulted in stimulation of the immune system. Specifically, necrotic cells release a number of immunostimulants such as HMGB1, purine metabolites, heat-shock proteins, adenine phosphate, and uric acid (Zong and Thompson, 2006). While massive necrosis such as that observed in tumor lysis syndrome can be life-threatening, this syndrome is fortunately restricted to poorly differentiated lymphomas and leukemias and although AG311 treatment increases necrosis *in vivo,* this involves only a portion of the tumor. Another argument against necrosis is that it can trigger the release of growth factors and cytokines leading to increased tumor growth (Hanahan and Weinberg, 2011). While not examined directly in this work, AG311 was active systemically against primary breast tumors and lung metastases *in vivo*, and its efficacy did not appear to decrease with multiple doses or as the tumors grew larger. This could be further

explored by measuring the release of pro-growth cytokines/growth factors from tumors exposed to AG311 and by assessing the “rebound” effect of prematurely withdrawing therapy on primary tumor and metastatic growth.

Therapeutically, it has been found that radiation-induced necrotic cell death can stimulate the immune system in a positive fashion to result in additional tumor cell kill via the bystander effect (Frey *et al.*, 2014). Further, the FDA approved anticancer agent topotecan, shown to result in necrotic cell death, increases levels of major histocompatibility complex class I (MHC I) proteins in breast cancer cells, leading to increased cytokine release, immune stimulation, and cancer death (Frey *et al.*, 2014). A tenet of photodynamic therapy (PDT) is its ability to induce cellular necrosis and acute inflammation locally in tumor tissue, and immune deficient animals do not seem to respond as well to PDT as their immune proficient counterparts (Henderson *et al.*, 2004; Brackett and Gollnick, 2011). Clinically, it has been suggested that antitumor therapy actually induces more necrosis than apoptosis, and that the degree of this necrosis is correlative with therapeutic outcome (Olofsson *et al.*, 2007; de Bruin and Medema, 2008). Thus, there is certainly a precedent for necrosis induction in cancer therapy.

AG311 is to our knowledge the first synthetic small molecule found to rapidly induce mitochondrial-related necrosis in tumor cells. Natural product toxins such as the kahalalides induce rapid cell death, but likely oligomerize directly to form pores in cellular membranes (Molina-Guijarro *et al.*, 2011). Honokiol is a small molecule lignan isolated from tree bark found to induce mitochondrial dysfunction and necrosis (L Li *et al.*, 2007). Certain small molecule chalcones have been found to induce rapid necrosis-like cell death called “methuosis”, or a buildup of large intracellular vacuoles (Overmeyer *et al.*, 2011). A methodical structure-activity analysis of AG311 is ongoing to better establish the basic pharmacophore conferring rapid induction of necrotic tumor cell death. These studies may also yield more active and tumor-selective agents and shed more light on

the cellular targets with which these agents might be interacting. Future studies will also examine the pharmacokinetic (PK) parameters of AG311 and related analogs; the *in vivo* efficacy of these agents in other resistant tumor types; and the *in vivo* efficacy and systemic toxicity in combination with FDA approved anticancer agents.

In conclusion, we have identified a small molecule capable of inducing rapid cellular necrosis through the mitochondria that is effective *in vitro* and *in vivo* against TNBC/BLBC primary tumors and metastases with no apparent toxicity. This agent may prove to be a first-in-class drug for the treatment of historically resistant solid tumors.

ACKNOWLEDGEMENT

We thank the Stephenson Cancer Center at the University of Oklahoma, Oklahoma City, OK for the use of the Cancer Tissue Pathology Core and the Functional Genomics Core, which provided photographic and imaging services.

AUTHORSHIP CONTRIBUTIONS

Participated in research design: Bastian, Bailey-Downs, Ihnat, Thorpe, Humphries, Gangjee

Conducted experiments: Bastian, Bailey-Downs, Thorpe, Disch, Vadvalkar, Devambatla

Contributed new reagents or analytic tools: Devambatla, Gangjee, Humphries, Henthorn

Performed data analysis: Bastian, Ihnat, Thorpe, Bailey-Downs

Wrote or contributed to the writing of the manuscript: Bastian, Ihnat, Bailey-Downs, Gangjee

REFERENCES

Aguer C, Gambarotta D, Mailloux RJ, Moffat C, Dent R, McPherson R, and Harper M-E (2011) Galactose enhances oxidative metabolism and reveals mitochondrial dysfunction in human primary muscle cells. *PLoS ONE* **6**:e28536.

American Cancer Society (2011) Cancer Facts & Figures 2011. **1**:1–60, Atlanta.

Bailey-Downs LC, Thorpe JE, Disch BC, Bastian A, Hauser PJ, Farasyn T, Berry WL, Hurst RE, and Ihnat MA (2014) Development and characterization of a preclinical model of breast cancer lung micrometastatic to macrometastatic progression. *PLoS ONE* **9**:e98624.

Barros LF, Kanaseki T, Sabirov R, Morishima S, Castro J, Bittner CX, Maeno E, Ando-Akatsuka Y, and Okada Y (2003) Apoptotic and necrotic blebs in epithelial cells display similar neck diameters but different kinase dependency. *Cell Death Differ* **10**:687–697.

Bonuccelli G, Tsirigos A, Whitaker-Menezes D, Pavlides S, Pestell RG, Chiavarina B, Frank PG, Flomenberg N, Howell A, Martinez-Outschoorn UE, Sotgia F, and Lisanti MP (2010) Ketones and lactate “fuel” tumor growth and metastasis: Evidence that epithelial cancer cells use oxidative mitochondrial metabolism. *Cell Cycle* **9**:3506–3514.

Brackett CM, and Gollnick SO (2011) Photodynamic therapy enhancement of anti-tumor immunity. *Photochem Photobiol Sci* **10**:649–652.

Chambers AF (2009) MDA-MB-435 and M14 Cell Lines: Identical but not M14 Melanoma? *Cancer Res* **69**:5292–5293.

Chan FK-M, Moriwaki K, and De Rosa MJ (2013) Detection of necrosis by release of lactate dehydrogenase activity. *Methods Mol Biol* **979**:65–70.

Chazotte B (2011) Labeling mitochondria with JC-1. *Cold Spring Harb Protoc* **9**:2011(9).

Choi K, Kim J, Kim GW, and Choi C (2009) Oxidative stress-induced necrotic cell death via mitochondira-dependent burst of reactive oxygen species. *Curr Neurovasc Res* **6**:213–222.

Clarke R, Leonessa F, Welch JN, and Skaar TC (2001) Cellular and molecular pharmacology of antiestrogen action and resistance. *J Pharmacol Exp Ther* **76**:71–84.

Costantini P, Jacotot E, and Decaudin D (2000) Mitochondrion as a novel target of anticancer chemotherapy. *J Natl Cancer Inst* **92**:1042–1053.

Dandajena TC, Ihnat MA, Disch B, Thorpe J, and Currier GF (2012) Hypoxia triggers a HIF-mediated differentiation of peripheral blood mononuclear cells into osteoclasts. *Orthod Craniofac Res* **15**:1–9.

de Bruin EC, and Medema JP (2008) Apoptosis and non-apoptotic deaths in cancer development and treatment response. *Cancer Treat Rev* **34**:737–749.

Dykens JA, Jamieson J, Marroquin L, Nadanaciva S, Billis PA, and Will Y (2008) Biguanide-induced mitochondrial dysfunction yields increased lactate production and cytotoxicity of aerobically-poised HepG2 cells and human hepatocytes in vitro. *Toxicol Appl Pharmacol* **233**:203–210.

Edinger AL, and Thompson CB (2004) Death by design: apoptosis, necrosis and autophagy. *Curr Opin Cell Biol* **16**:663–669.

Epps DE, Wolfe ML, and Groppi V (1994) Characterization of the steady-state and dynamic fluorescence properties of the potential-sensitive dye *bis*-(1,3-dibutylbarbituric acid)trimethine oxonol ($Dibac_4(3)$) in model systems and cells. *Chem Phys Lipids* **69**:137–150.

Frey B, Rubner Y, Kulzer L, Werthmöller N, Weiss E-M, Fietkau R, and Gaipl US (2014) Antitumor immune responses induced by ionizing irradiation and further immune stimulation. *Cancer Immunol Immunother* **63**:29–36.

Gangjee A, Zaware N, Raghavan S, Ihnat M, Shenoy S, and Kisliuk RL (2010) Single agents with designed combination chemotherapy potential: synthesis and evaluation of substituted pyrimido[4,5-b]indoles as receptor tyrosine kinase and thymidylate synthase inhibitors and as antitumor agents. *J Med Chem* **53**:1563–1578.

García-Rivas G de J, Carvajal K, Correa F, and Zazueta C (2006) Ru360, a specific mitochondrial calcium uptake inhibitor, improves cardiac post-ischaemic functional recovery in rats in vivo. *Br J Pharmacol* **149**:829–837.

Golstein P, and Kroemer G (2007) Cell death by necrosis: towards a molecular definition. *Trends Biochem Sci* **32**:37–43.

Gradishar WJ, Anderson BO, Blair SL, Burstein HJ, Cyr A, Elias AD, Farrar WB, Forero A, Giordano SH, Goldstein LJ, Hayes DF, Hudis CA, Isakoff SJ, Ljung B-ME, Marcom PK, Mayer IA, McCormick B, Miller RS, Pegram M, Pierce LJ, Reed EC, Salerno KE, Schwartzberg LS, Smith ML, Soliman H, Somlo G, Ward JH, Wolff AC, Zellars R, Shead DA, and Kumar R (2014) NCCN Clinical Practice and Guidelines in Oncology (NCCN Guidelines) Breast cancer version 3.2014. *J Natl Compr Canc Netw* **12**:542–590.

Hamahata K, Adachi S, Matsubara H, Okada M, Imai T, Watanabe K-I, Toyokuni S-Y, Ueno M, Wakabayashi S, Katanosaka Y, Akiba S, Kubota M, and Nakahata T (2005) Mitochondrial dysfunction is related to necrosis-like programmed cell death induced by A23187 in CEM cells. *Eur J Pharmacol* **516**:187–196.

Hanahan D, and Weinberg RA (2011) Hallmarks of cancer: the next generation. *Cell* **144**:646–674.

Henderson BW, Gollnick SO, Snyder JW, and Busch TM (2004) Choice of oxygen-conserving treatment regimen determines the inflammatory response and outcome of photodynamic therapy of tumors. *Cancer Res* **64**:2120–2126.

Ihnat MA, Nervi AM, Anthony SP, Kaltreider RC, Warren AJ, Pesce CA, Davis SA, Lariviere JP, and Hamilton JW (1999) Effects of mitomycin C and carboplatin pretreatment on multidrug resistance-associated P-glycoprotein expression and on subsequent suppression of tumor growth by doxorubicin and paclitaxel in human metastatic breast cancer xenografted nude mice. *Oncol Res* **11**:303–310.

Kamat CD, Green DE, Warnke L, Thorpe JE, Ceriello A, and Ihnat MA (2007) Mutant p53 facilitates pro-angiogenic, hyperproliferative phenotype in response to chronic relative hypoxia. *Cancer Lett* **249**:209–219.

Kinnally KW, Peixoto PM, Ryu S-Y, and Dejean LM (2011) Is mPTP the gatekeeper for necrosis, apoptosis, or both? *Biochim Biophys Acta* **1813**:616–622.

Lena A, Rechichi M, Salvetti A, Bartoli B, Vecchio D, Scarcelli V, Amoroso R, Benvenuti L, Gagliardi R, Gremigni V, and Rossi L (2009) Drugs targeting the mitochondrial pore act as cytotoxic and cytostatic agents in temozolomide-resistant glioma cells. *J Transl Med* **7**:13.

Li L, Han W, Gu Y, Qiu S, Lu Q, Jin J, Luo J, and Hu X (2007) Honokiol induces a necrotic cell death through the mitochondrial permeability transition pore. *Cancer Res* **67**:4894–4903.

Li YC, Fung KP, Kwok TT, Lee CY, Suen YK, and Kong SK (2004) Mitochondria-targeting drug oligomycin blocked P-glycoprotein activity and triggered apoptosis in doxorubicin-resistant HepG2 cells. *Chemotherapy* **50**:55–62.

Molina-Guijarro JM, Macías Á, García C, Muñoz E, García-Fernández LF, David M, Núñez L, Martínez-Leal JF, Moneo V, Cuevas C, Lillo MP, Villalobos Jorge C, Valenzuela C, and Galmarini CM (2011) Irvalec inserts into the plasma membrane causing rapid loss of integrity and necrotic cell death in tumor cells. *PLoS ONE* **6**:e19042.

Ohashi K, Maruvka YE, Michor F, and Pao W (2013) Epidermal growth factor receptor tyrosine kinase inhibitor-resistant disease. *J Clin Oncol* **31**:1070–1080.

Olofsson MH, Ueno T, Pan Y, Xu R, Cai F, van der Kuip H, Muerdter TE, Sonnenberg M, Aulitzky WE, Schwarz S, Andersson E, Shoshan MC, Havelka AM, Toi M, and Linder S (2007) Cytokeratin-18 is a useful serum biomarker for early determination of response of breast carcinomas to chemotherapy. *Clin Cancer Res* **13**:3198–3206.

Overmeyer JH, Young AM, Bhanot H, and Maltese WA (2011) A chalcone-related small molecule that induces methuosis, a novel form of non-apoptotic cell death, in glioblastoma cells. *Mol Cancer* **10**:69.

Perry SW, Norman JP, Barbieri J, Brown EB, and Gelbard HA (2011) Mitochondrial membrane potential probes and the proton gradient: a practical usage guide. *BioTechniques* **50**:98–115.

Reagan-Shaw S, Nihal M, and Ahmad N (2008) Dose translation from animal to human studies revisited. *FASEB J* **22**:659–661.

Ricci MS, and Zong W-X (2006) Chemotherapeutic approaches for targeting cell death pathways. *Oncologist* **11**:342–357.

Ryter SW, Kim HP, Hoetzel A, Park JW, Nakahira K, Wang X, and Choi AMK (2007) Mechanisms of cell death in oxidative stress. *Antioxid Redox Signal* **9**:49–89.

Sanchez-Alvarez R, Martinez-Outschoorn UE, Lamb R, Hulit J, Howell A, Gandara R, Sartini M, Rubin E, Lisanti MP, and Sotgia F (2013) Mitochondrial dysfunction in breast cancer cells prevents tumor growth: understanding chemoprevention with metformin. *Cell Cycle* **12**:172–182.

Scaffidi P, Misteli T, and Bianchi ME (2002) Release of chromatin protein HMGB1 by necrotic cells triggers inflammation. *Nature* **418**:191–195.

Smith AR, Shenvi SV, Widlansky M, Suh JH, and Hagen TM (2004) Lipoic Acid as a Potential Therapy for Chronic Diseases Associated with Oxidative Stress. *Curr Med Chem* **11**:1135–1146.

Sotgia F, Whitaker-Menezes D, Martinez-Outschoorn UE, Flomenberg N, Birbe RC, Witkiewicz AK, Howell A, Philp NJ, Pestell RG, and Lisanti MP (2012) Mitochondrial metabolism in cancer metastasis: visualizing tumor cell mitochondria and the "reverse Warburg effect" in positive lymph node tissue. *Cell Cycle* **11**:1445–1454.

Valencia T, Kim JY, Abu-Baker S, Moscat-Pardos J, Ahn CS, Reina-Campos M, Duran A, Castilla EA, Metallo CM, Diaz-Meco MT, and Moscat J (2014) Metabolic Reprogramming of Stromal Fibroblasts through p62-mTORC1 Signaling Promotes

Inflammation and Tumorigenesis. *Cancer Cell* **26**:121–135.

Vanden Berghe T, Linkermann A, Jouan-Lanhouet S, Walczak H, and Vandenabeele P (2014) Regulated necrosis: the expanding network of non-apoptotic cell death pathways. *Nat Rev Mol Cell Biol* **15**:135–147.

Whitaker-Menezes D, Martinez-Outschoorn UE, Flomenberg N, Birbe RC, Witkiewicz AK, Howell A, Pavlides S, Tsirigos A, Ertel A, Pestell RG, Broda P, Minetti C, Lisanti MP, and Sotgia F (2011) Hyperactivation of oxidative mitochondrial metabolism in epithelial cancer cells in situ: Visualizing the therapeutic effects of metformin in tumor tissue. *Cell Cycle* **10**:4047–4064.

Witkiewicz AK, Whitaker-Menezes D, Dasgupta A, Philp NJ, Lin Z, Gandara R, Sneddon S, Martinez-Outschoorn UE, Sotgia F, and Lisanti MP (2012) Using the “reverse Warburg effect” to identify high-risk breast cancer patients: Stromal MCT4 predicts poor clinical outcome in triple-negative breast cancers. *Cell Cycle* **11**:1108–1117.

Yoo J-O, and Ha K-S (2012) New insights into the mechanisms for photodynamic therapy-induced cancer cell death. *Int Rev Cell Mol Biol* **295**:139–174.

Yuan N, Meng M, Liu C, Feng L, Hou L, Ning Q, Xin G, Pei L, Gu S, Li X, and Zhao X (2014) Clinical characteristics and prognostic analysis of triple-negative breast cancer patients. *Mol Clin Onc* **2**:245–251.

Zhang X, Fryknäs M, Hernlund E, Fayad W, De Milito A, Olofsson MH, Gogvadze V, Dang L, Påhlman S, Schughart LAK, Rickardson L, D'Arcy P, Gullbo J, Nygren P, Larsson R, and Linder S (2014) Induction of mitochondrial dysfunction as a strategy for targeting tumour cells in metabolically compromised microenvironments. *Nat Commun* **5**:3295.

Zhao Y, Butler EB, and Tan M (2013) Targeting cellular metabolism to improve cancer therapeutics. *Cell Death Dis* **4**:e532.

Zhou H, Zhang B, Zheng J, Yu M, Zhou T, Zhao K, Jia Y, Gao X, Chen C, and Wei T (2014) The inhibition of migration and invasion of cancer cells by graphene via the impairment of mitochondrial respiration. *Biomaterials* **35**:1597–1607.

Zong W-X, and Thompson CB (2006) Necrotic death as a cell fate. *Genes Dev* **20**:1–15.

Zong WX, Ditsworth D, Bauer DE, Wang ZQ, and Thompson CB (2004) Alkylating DNA damage stimulates a regulated form of necrotic cell death. *Genes Dev* **18**:1272–1282.

FOOTNOTES

This work was supported in part, by a grant from the National Institutes of Health, National Cancer Institute [Grant CA136944] (A.G., M.A.I.), by College of Pharmacy startup funds (M.A.I.) and by an Institutional Development Award (IDeA) from the National Institute of General Medical Sciences of the National Institutes of Health under [Grant P20GM103639] (Stephenson Cancer Center Core).

FINANCIAL DISCLOSURE

BCD and LBD are employees of DormaTarg, have no financial interest in the company, and DormaTarg has no financial interest in the work presented within.

JPET Fast Forward. Published on February 26, 2015 as DOI: 10.1124/jpet.114.220335
This article has not been copyedited and formatted. The final version may differ from this version.

FIGURE LEGENDS

Figure 1. AG311 preferentially induces rapid cell death and selective membrane permeability in breast cancer cells.

A) Structure of AG311. **B)** IC_{50} values for AG311 with different cell lines. Viability was determined by PrestoBlue fluorescence after 48 hours of treatment. **C)** Dose-response curves of AG311 on TNBC cell lines. **D)** Brightfield (BF) and fluorescent time course images of MDA-MB-435 cells exposed to AG311 (20 µM) in the presence of SYTOX Green. Arrows indicate cellular swelling and large blebbing. **E)** Membrane permeability time course in MDA-MB-435 cells and **F)** HUVEC treated with AG311 in the presence of SYTOX green (n = 9). **G)** Mixed cell culture of HDF (labeled green with CellTracker Green) and MDA-MB-435 cells (labeled red with CellTracker Red) treated with AG311 (20 µM) in the presence of SYTOX blue. **H)** Viability time course of AG311-treated MDA-MB-435 cells as determined with PrestoBlue. All data are representative of three to six independent experiments.

Figure 2. AG311 induces characteristics of necrotic cell death.

A) Lactate dehydrogenase (LDH) release from AG311-treated MDA-MB-435 cells (n=4). **B)** Average measurement of nuclear diameter of AG311-treated (25 µM) MDA-MB-435 cells for 20 minutes (n = 8 - 11). **C)** Time course of ATP levels in AG311-treated MDA-MB-435 cells (n = 4 - 5). **D)** Immunofluorescence images of MDA-MB-435 cells treated with AG311 (25 µM) for 20 minutes. Images representative of three separate experiments. **E**) Immunoblot of HMGB1 levels in cell lysate (cytosolic fraction) collected form AG311-treated (25 µM) MDA-MB-435 cells and solvent control. Graphs show quantification of HMGB1 levels normalized to vinculin.

Figure 3. AG311 induces intracellular calcium increase and membrane depolarization.

A) MDA-MB-435 cells treated with AG311 (20 μM) in the presence of Fluo-4 calcium indicator and propidium iodide (PI) (left panel). Cell tracings of treated cells (right panel); n = 6 cells. **B)** Cells were treated with AG311 (20 μM) in calcium containing or calcium free media with SYTOX Green. **C)** Viability of cells treated with AG311 after pretreatment with BAPTA-AM. The viability was assessed by PrestoBlue after 24 hours of treatment. **D)** MDA-MB-435 cells were loaded with $DiBAC_4(3)$ and exposed to AG311 or control. Data are mean fluorescence intensities of cell traces (n=6 cells). $DiBAC_4(3)$ fluorescence intensity correlates with membrane potential, while propidium iodide (PI) fluorescence intensity correlates with membrane permeabilization. Data are representative of three independent experiments.

Figure 4. Effect of AG311 on mitochondria.

A) MDA-MB-435 cells (used throughout) were treated with AG311 or solvent control (0.2% DMSO) in the presence of TMRM and imaged at 40x (left panel) or represented as cell tracings at multiple doses of AG311 (right panel). Statistical analysis was performed with two-way ANOVA/repeated measures post-test. **B)** TMRM-loaded MDA-MB-435 cells were analyzed for fluorescence intensity with flow cytometry kinetics. Arrow indicates time of addition of solvent control (0.2% DMSO) or AG311 (20 μM) to the cell suspension at 5 minutes. **C)** Flow cytometric analysis of AG311-treated (20 μM) or untreated cells after JC-1 loading. **D)** Additional time points of percentage of cells treated with AG311 present in quadrant 2 (Q2) in JC-1 flow cytometry plot.

Figure 5. Partial prevention of AG311-induced cell death by Ru360, lipoic acid, and galactose.

A) Viability of AG311-treated (20 μM) cells after pretreatment with Ru360, measured with PrestoBlue (24 hr) or **(B)** membrane permeability assessed by SYTOX Green fluorescence. Statistical analysis was performed with two-way ANOVA/repeated measures post-test. The *p*-values for AG311 alone compared to AG311 + Ru360 at the different time points are at least < 0.05 after 60 minutes of treatment and onward. **C)** Viability assessment of cells cultured in glucose (25 mM) or galactose (10 mM) supplemented DMEM for 5 days, and then treated with AG311. **D)** Superoxide production was determined by MitoSOX fluorescence (red) and membrane permeability determined by SYTOX Green (black) in AG311-treated (20 μM) cells (n = 5). **E)** Plate reader analysis of mitochondrial superoxide production in response to AG311 (20 μM) Statistical analysis was performed with two-way ANOVA/repeated measures post-test. **F)** Viability of cells treated with AG311 with or without lipoic acid. Viability was assessed with Presto Blue after 24 hours.

Figure 6. AG311 inhibits breast cancer cell migration

Cells (4T1-luc2-GFP) were treated with AG311 (0, 8, 10, 12, 14 μM) or latrunculin A (Lat, 0.25 μM) for 30 hours. **A)** Cells were labeled with calcein-AM and cell migration measured from images. **B)** Representative images. Dotted line indicates initial hole in the cell layer. **C)** Cells were subjected to PrestoBlue for viability determination. The treatment did not reduce viability. **D, E & F)** Cells were treated as above, with the exception that cells were pretreated with mitomycin C (10 μM) for 2 hours prior to treatment. Data are representative of three independent experiments.

Figure 7. AG311 increases necrosis in orthotopic breast tumors

A) 4T1 tumor-bearing BALB/cJ mice were treated intratumorally with AG311 or solvent control once daily for two days. Quantification of necrotic area from H&E sections. Data

are means (n = 9 - 11 tumors). **B)** Representative tumor sections from mice treated with AG311 or control.

Figure 8. AG311 retards tumor growth and reduces metastasis with low systemic toxicity in orthotopic breast cancer.

A) MDA-MB-435 GFP tumor growth curve in an orthotopic xenograft mouse model. Tumor bearing NCr nu/nu athymic mice were treated with control, doxorubicin (dox) (15 mg/kg, weekly), AG311 (45 mg/kg, twice weekly) and tumor volumes assessed (two-way ANOVA repeated measures post-test). **B)** Visible GFP lung metastatic cell count at the end of the experiment. **C)** Mouse weight change at the end of the experiment (n = 5). **D)** 4T1-luc2-GFP tumor bearing BALB/cJ mice were treated with AG311 (50 mg/kg, twice weekly), docetaxel (dct) (15 mg/kg, weekly), or solvent control and tumor volume assessed (two-way ANOVA/repeated measures post-test). **E)** GFP-positive lung metastatic cell count normalized to solvent control. **F)** Mouse weights are shown in percentage change at day 32 over starting weight (n = 4 - 6).

Figure 9. Events of AG311-induced cell death.

Summary scheme of the timing of cellular events occurring during AG311-induced cell death (20 µM).

Figure 1.

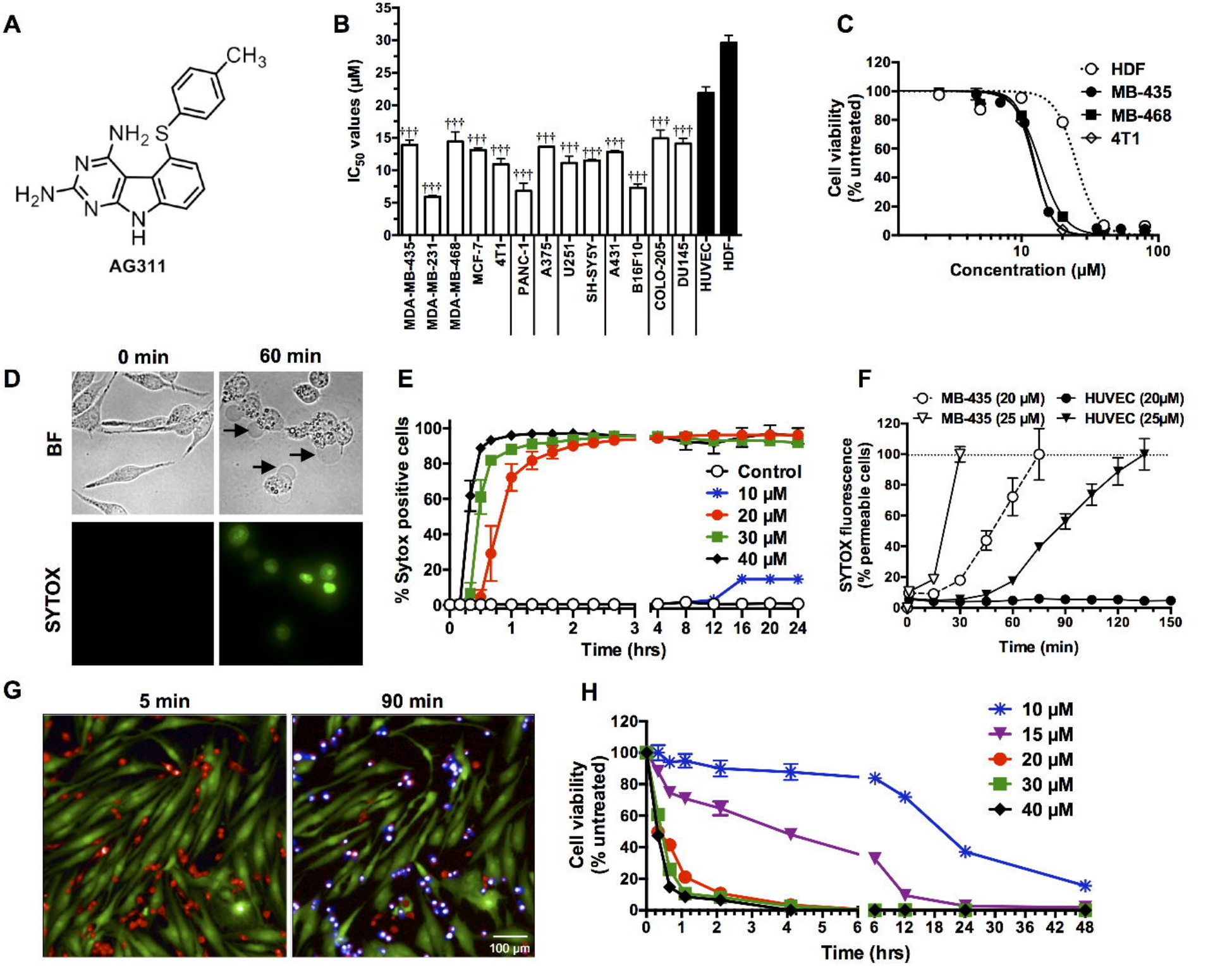
A
AG311
B
IC50 values (μM)
MDA-MB-435
MDA-MB-231
MDA-MB-468
MCF-7
4T1
PANC-1
A375
U251
SH-SY5Y
A431
B16F10
COLO-205
DU145
HUVEC
HDF
C
Cell viability (% untreated)
Concentration (μM)
HDF
MB-435
MB-468
4T1
D
0 min
60 min
BF
SYTOX
E
% Sytox positive cells
Time (hrs)
Control
10 μM
20 μM
30 μM
40 μM
F
MB-435 (20 μM)
MB-435 (25 μM)
HUVEC (20μM)
HUVEC (25μM)
SYTOX fluorescence (% permeable cells)
Time (min)
G
5 min
90 min
100 μm
H
Cell viability (% untreated)
Time (hrs)
10 μM
15 μM
20 μM
30 μM
40 μM

Figure 2.

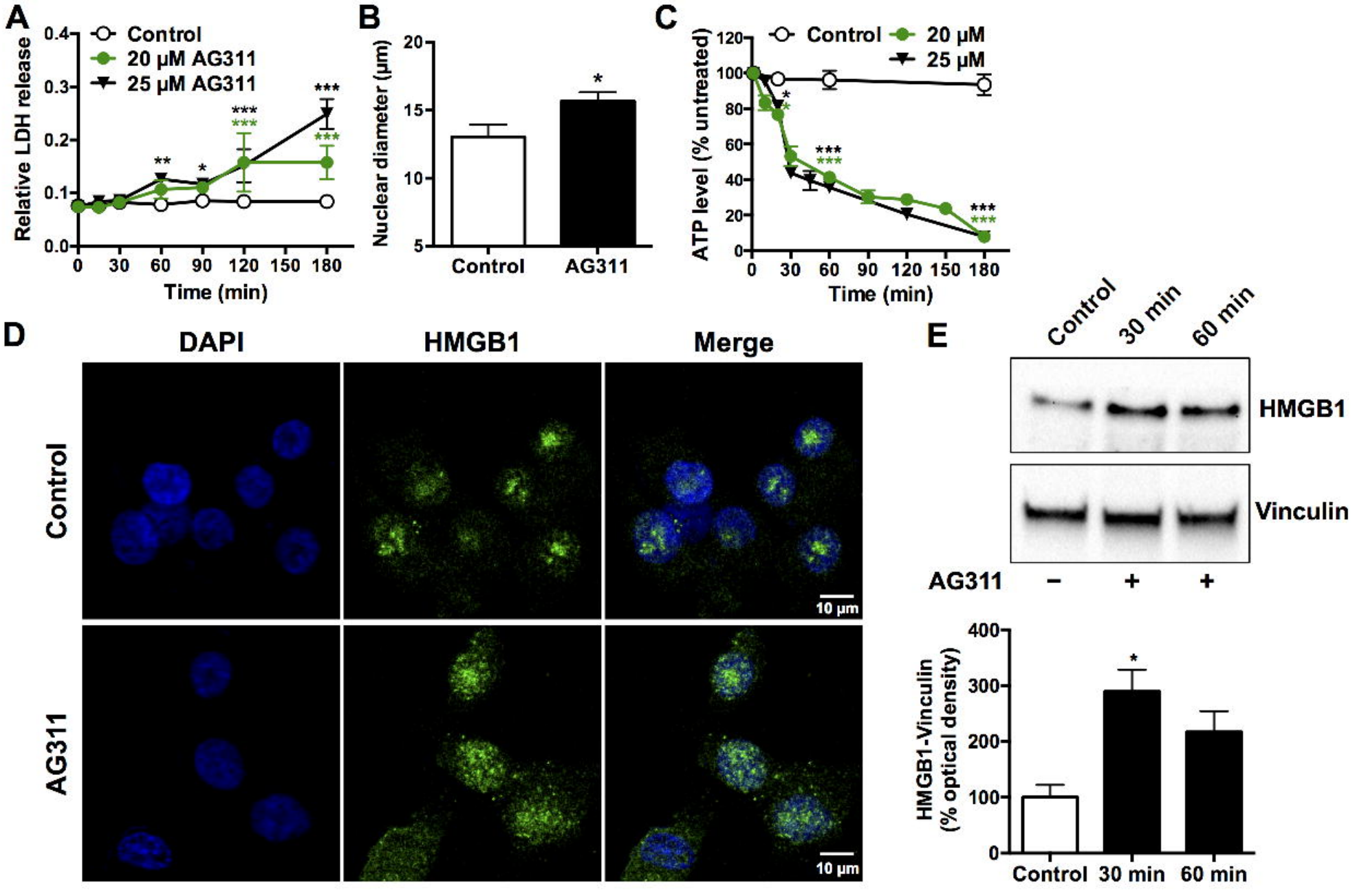
A
Relative LDH release
Control
20 μM AG311
25 μM AG311
Time (min)
B
Nuclear diameter (μm)
Control
AG311
C
ATP level (% untreated)
Control
20 μM
25 μM
Time (min)
D
DAPI
HMGB1
Merge
Control
AG311
10 μm
E
Control
30 min
60 min
HMGB1
Vinculin
AG311
HMGB1-Vinculin (% optical density)
Control
30 min
60 min

Figure 3.

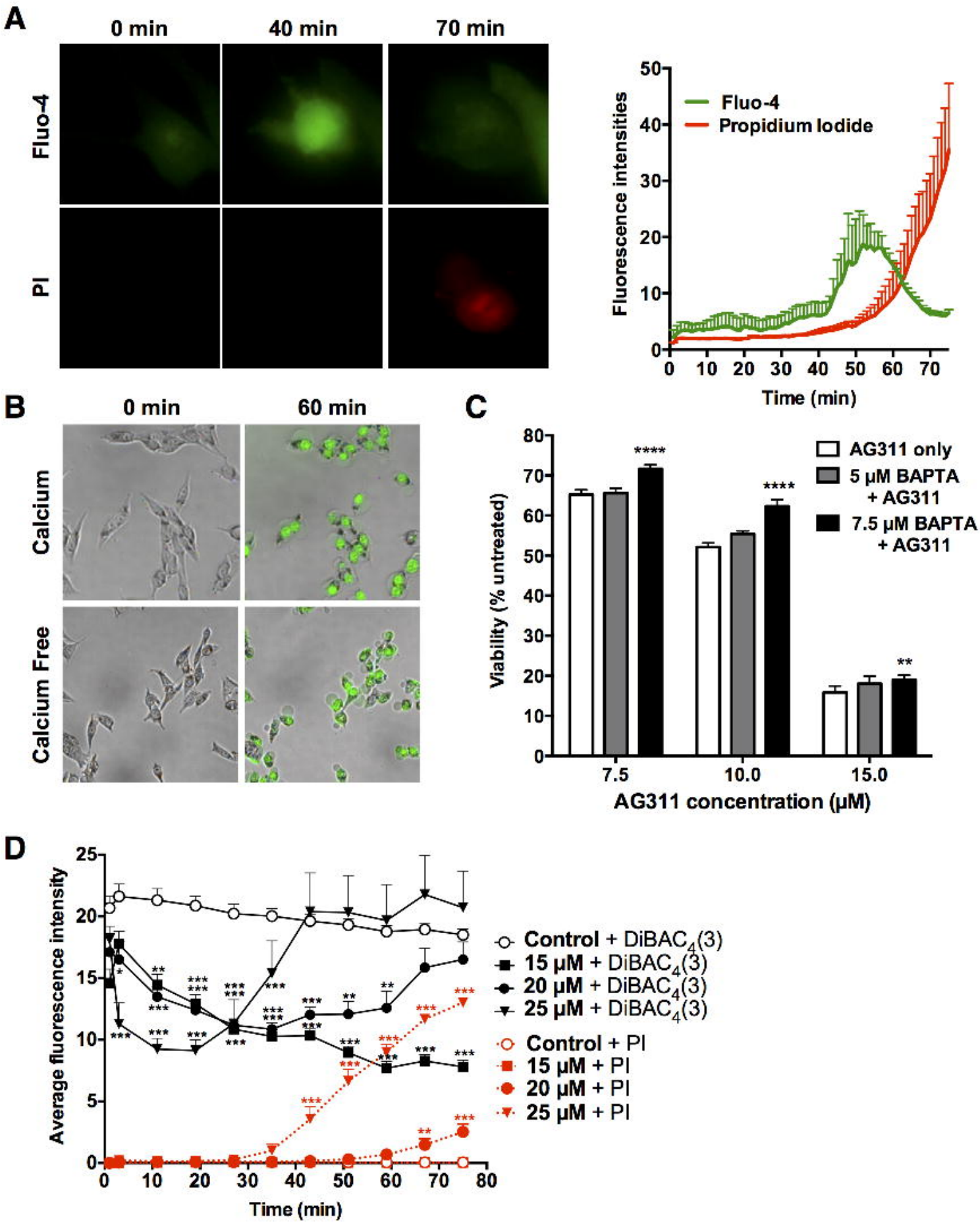
A
0 min
40 min
70 min
Fluo-4
PI
Fluo-4
Propidium Iodide
Fluorescence intensities
Time (min)
B
0 min
60 min
Calcium
Calcium Free
C
AG311 only
5 μM BAPTA + AG311
7.5 μM BAPTA + AG311
Viability (% untreated)
AG311 concentration (μM)
D
Average fluorescence intensity
Time (min)
Control + DiBAC4(3)
15 μM + DiBAC4(3)
20 μM + DiBAC4(3)
25 μM + DiBAC4(3)
Control + PI
15 μM + PI
20 μM + PI
25 μM + PI

Figure 4.

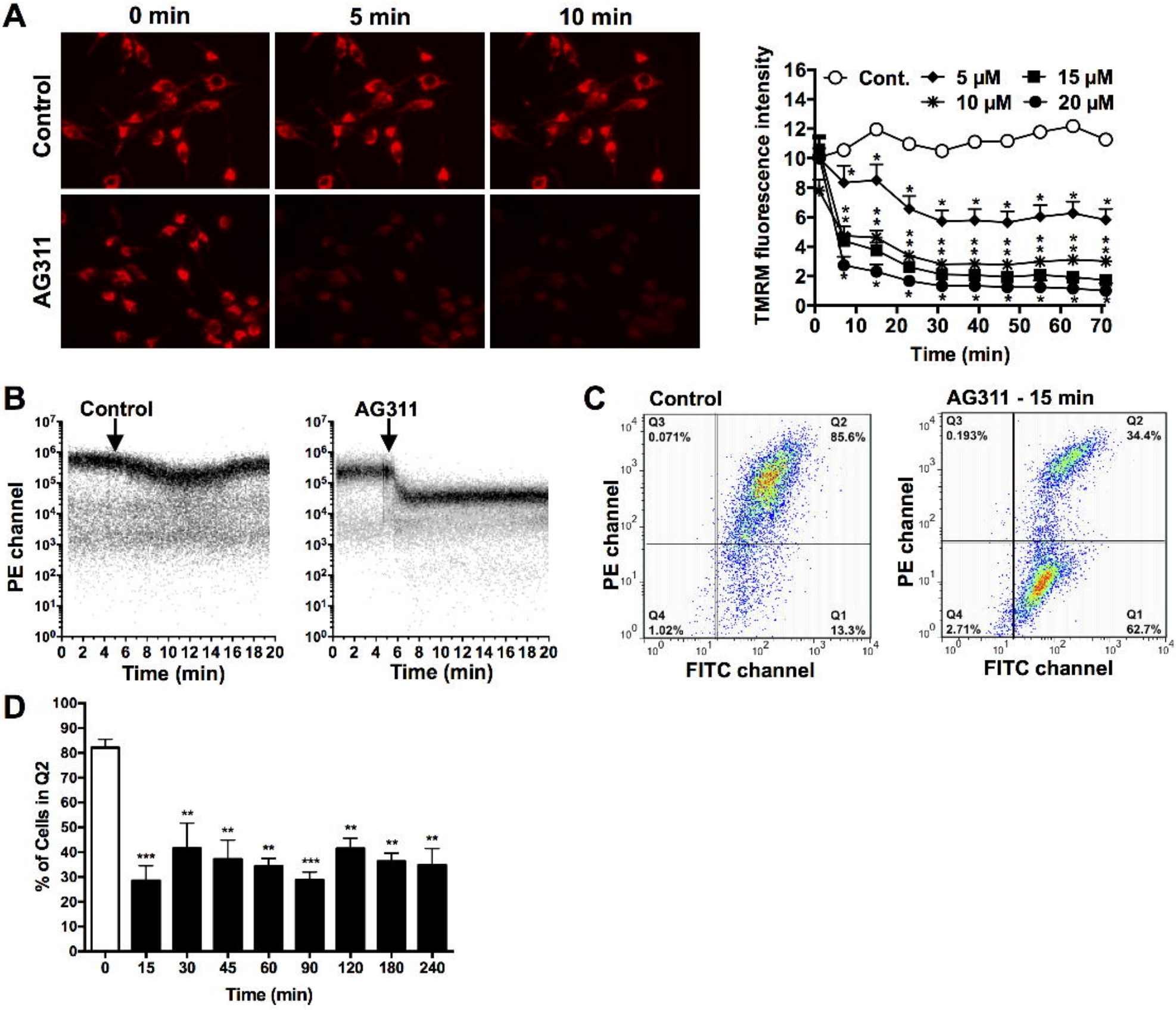
A
0 min
5 min
10 min
Control
AG311
TMRM fluorescence intensity
Cont.
5 μM
15 μM
10 μM
20 μM
Time (min)
B
Control
AG311
PE channel
Time (min)
C
Control
AG311 - 15 min
Q3
0.071%
Q2
85.6%
Q4
1.02%
Q1
13.3%
Q3
0.193%
Q2
34.4%
Q4
2.71%
Q1
62.7%
PE channel
FITC channel
D
% of Cells in Q2
Time (min)

Figure 5.

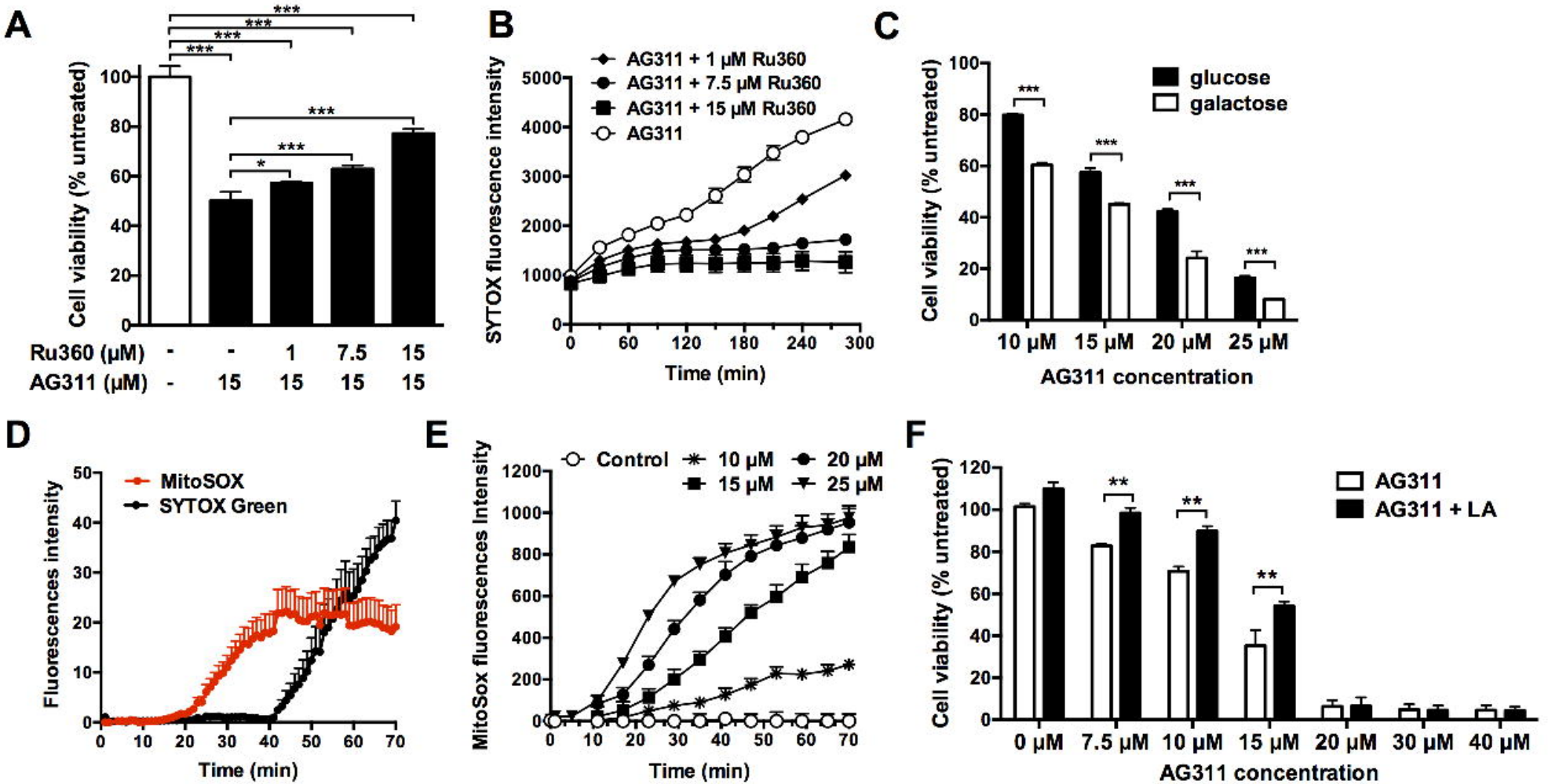
A
Cell viability (% untreated)
Ru360 (μM) - - 1 7.5 15
AG311 (μM) - 15 15 15 15
B
AG311 + 1 μM Ru360
AG311 + 7.5 μM Ru360
AG311 + 15 μM Ru360
AG311
SYTOX fluorescence intensity
Time (min)
C
glucose
galactose
Cell viability (% untreated)
10 μM 15 μM 20 μM 25 μM
AG311 concentration
D
MitoSOX
SYTOX Green
Fluorescences intensity
Time (min)
E
Control 10 μM 20 μM
15 μM 25 μM
MitoSox fluorescences Intensity
Time (min)
F
AG311
AG311 + LA
Cell viability (% untreated)
0 μM 7.5 μM 10 μM 15 μM 20 μM 30 μM 40 μM
AG311 concentration

Figure 6.

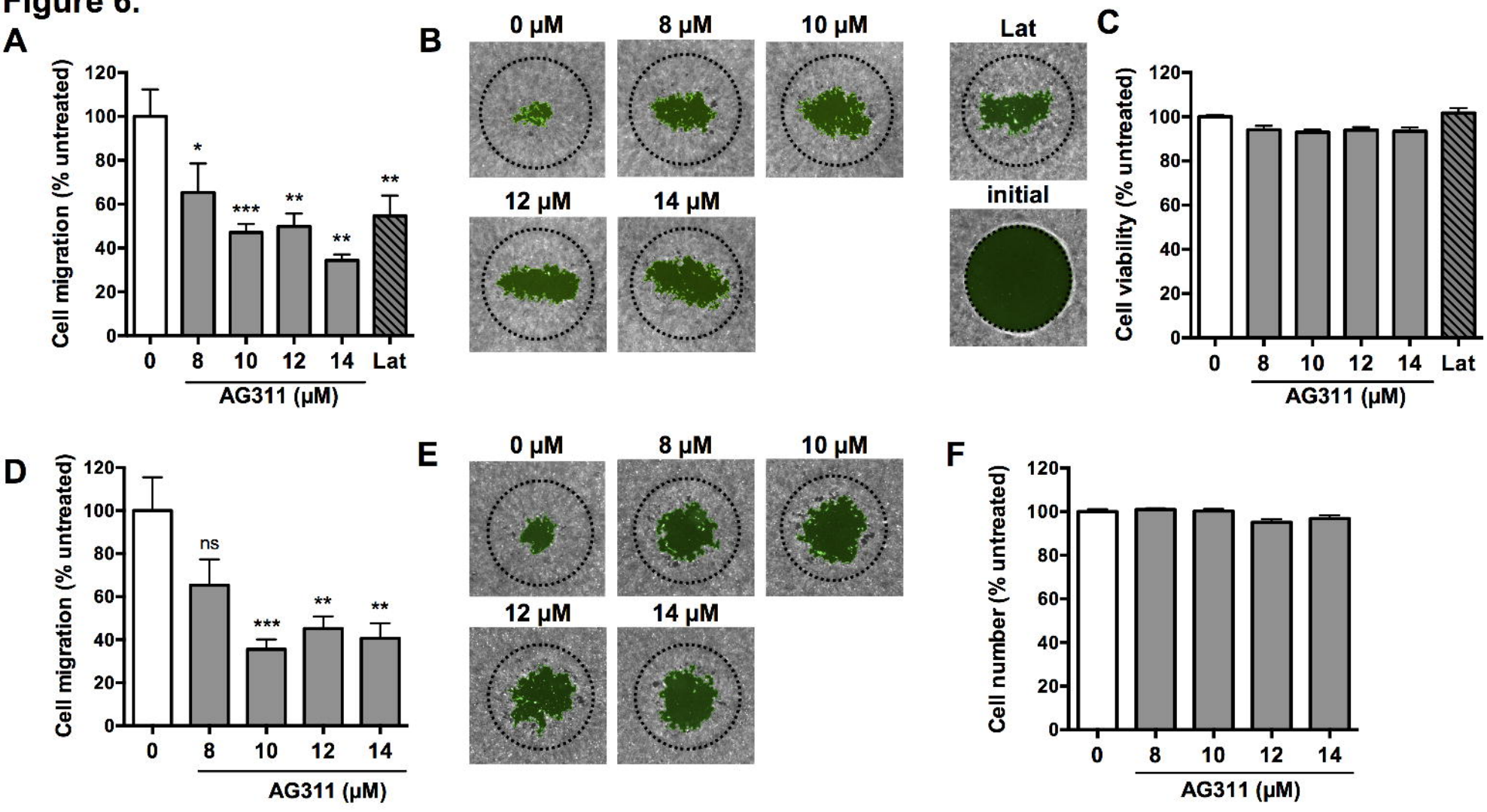
A
Cell migration (% untreated)
120
100
80
60
40
20
0
*
***
**
**
**
0
8
10
12
14
Lat
AG311 (μM)
B
0 μM
8 μM
10 μM
12 μM
14 μM
Lat
initial
C
Cell viability (% untreated)
120
100
80
60
40
20
0
0
8
10
12
14
Lat
AG311 (μM)
D
Cell migration (% untreated)
120
100
80
60
40
20
0
ns
***
**
**
0
8
10
12
14
AG311 (μM)
E
0 μM
8 μM
10 μM
12 μM
14 μM
F
Cell number (% untreated)
120
100
80
60
40
20
0
0
8
10
12
14
AG311 (μM)

Figure 7.

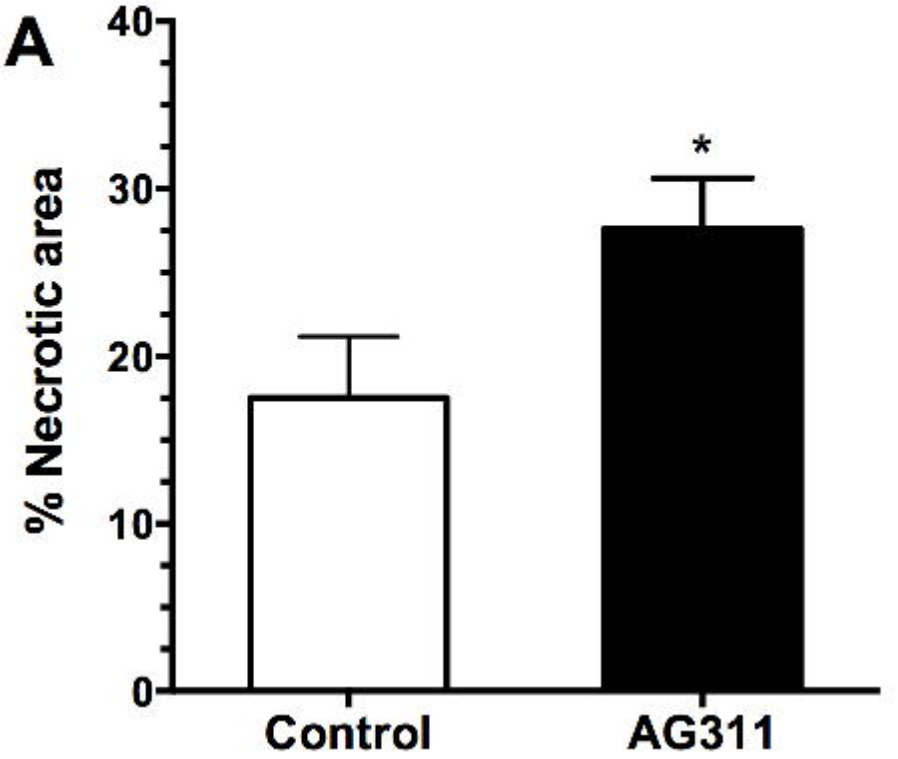
A
40
30
20
10
0
% Necrotic area
*
Control
AG311

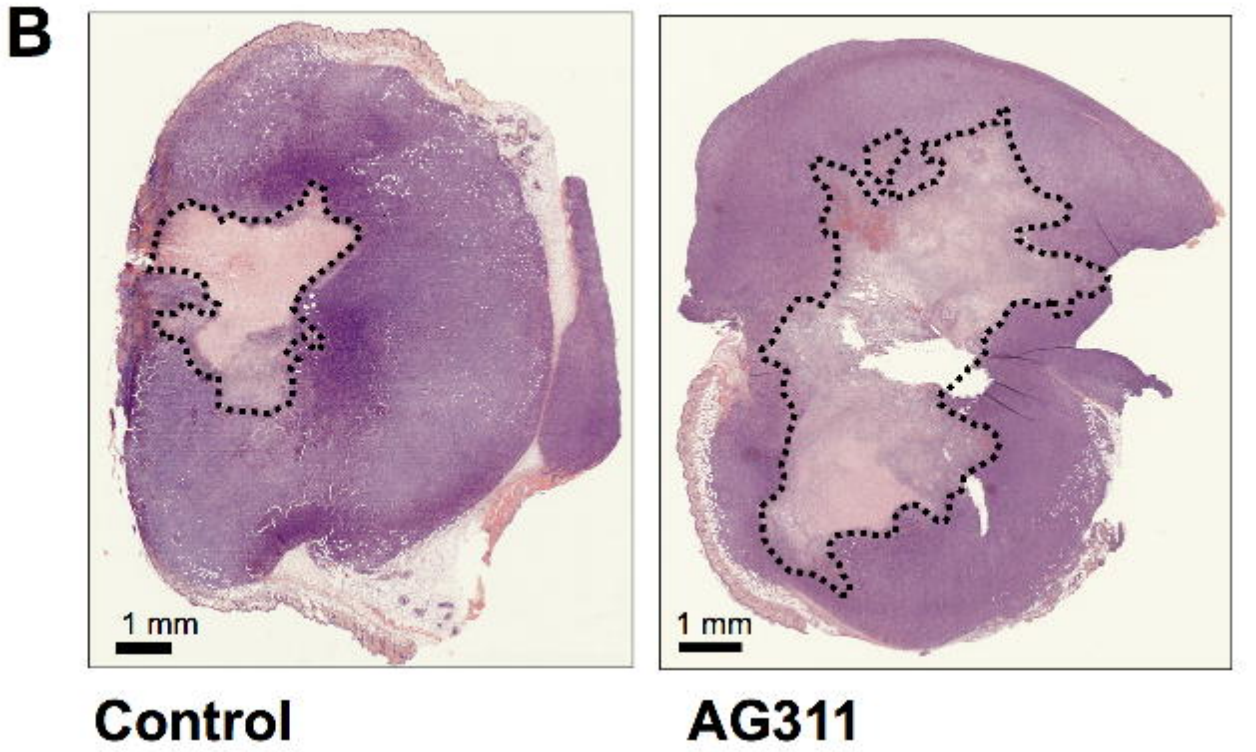
B
1 mm
1 mm
Control
AG311

Figure 8.

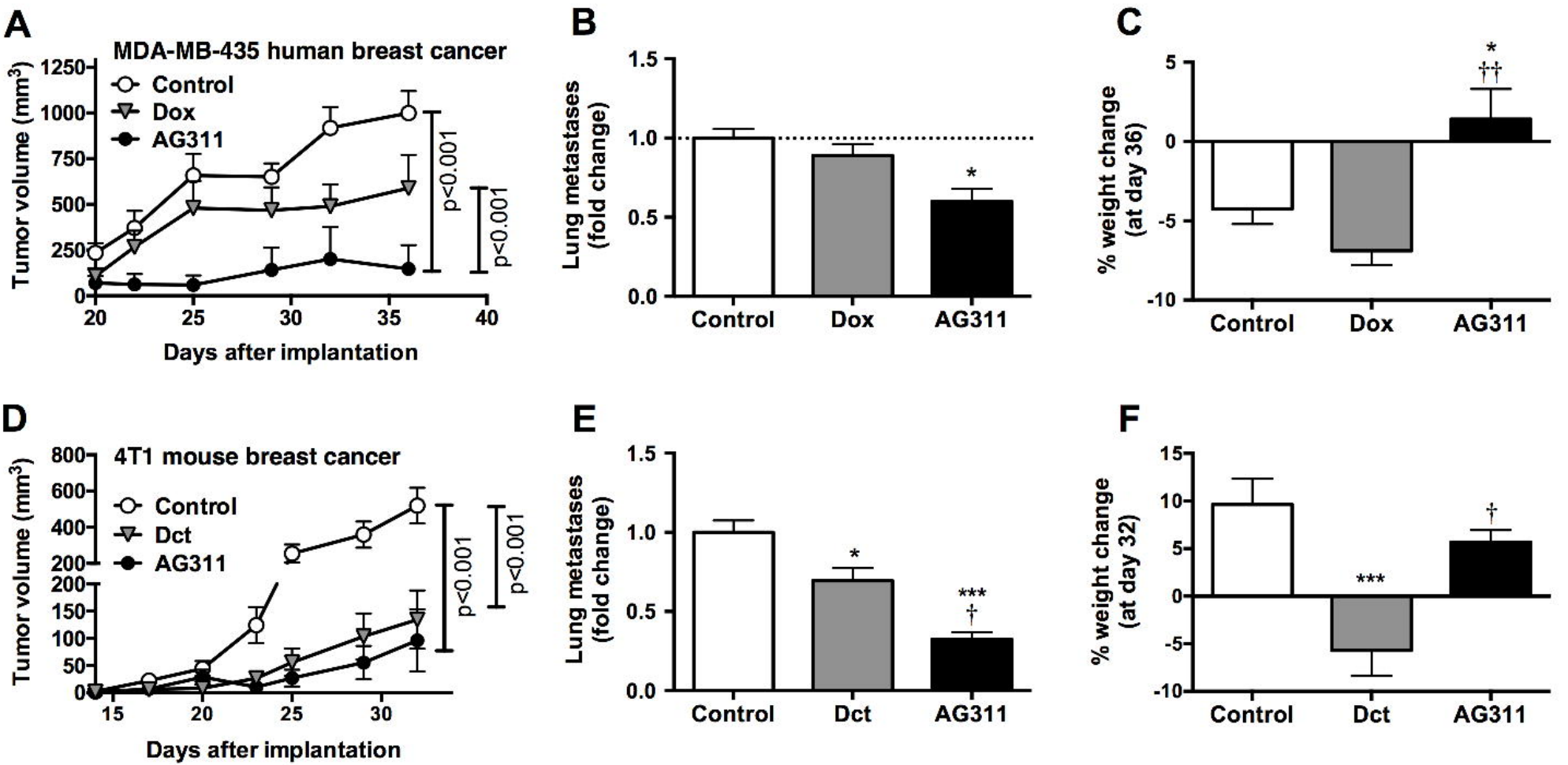
A
MDA-MB-435 human breast cancer
Control
Dox
AG311
Tumor volume (mm3)
1250
1000
750
500
250
0
20
25
30
35
40
Days after implantation
p<0.001
p<0.001
B
Lung metastases (fold change)
1.5
1.0
0.5
0.0
Control
Dox
AG311
*
C
% weight change (at day 36)
5
0
-5
-10
Control
Dox
AG311
*
††
D
4T1 mouse breast cancer
Control
Dct
AG311
Tumor volume (mm3)
800
600
400
200
200
150
100
50
0
15
20
25
30
Days after implantation
p<0.001
p<0.001
E
Lung metastases (fold change)
1.5
1.0
0.5
0.0
Control
Dct
AG311
*
***
†
F
% weight change (at day 32)
15
10
5
0
-5
-10
Control
Dct
AG311
***
†

Figure 9.

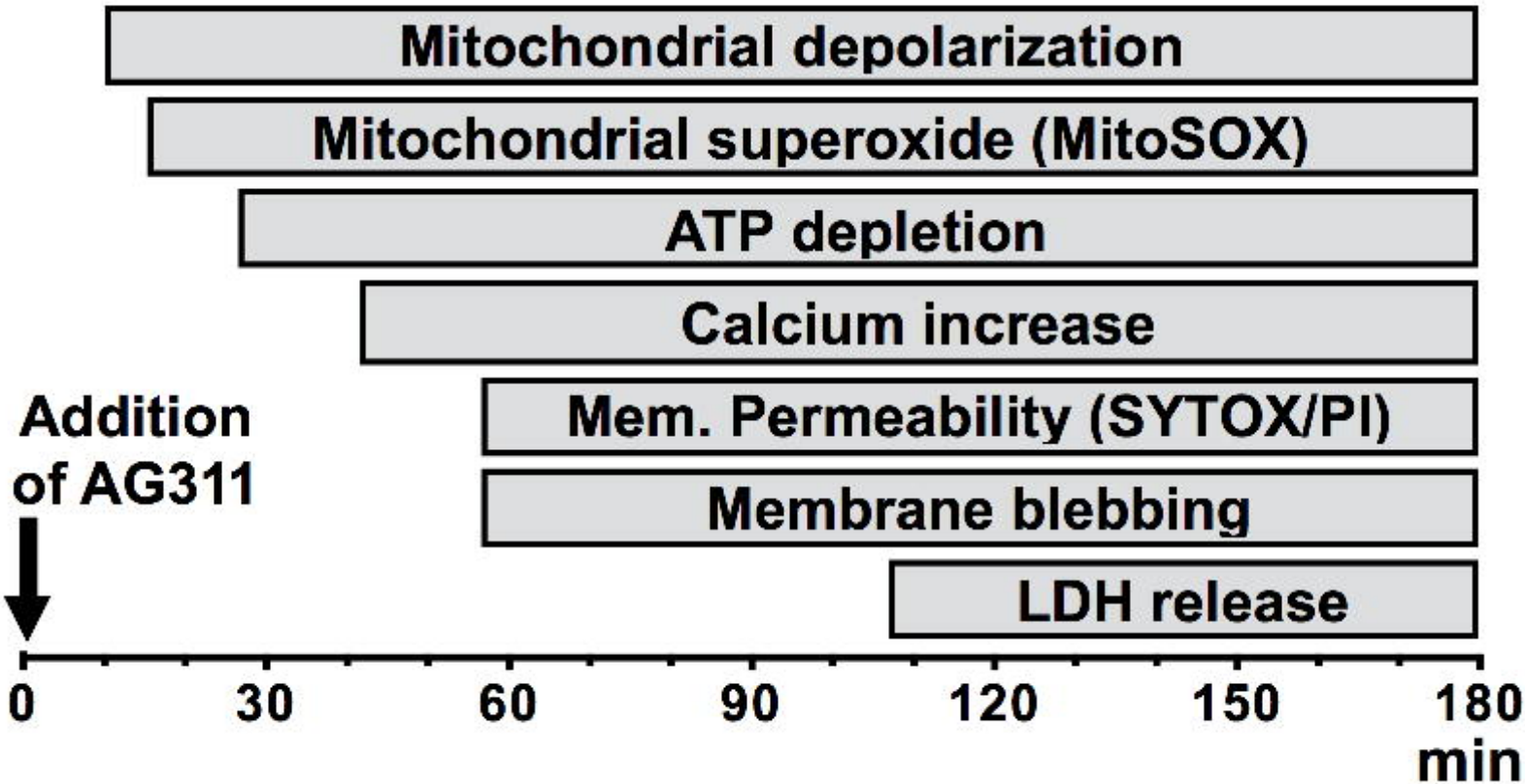
Mitochondrial depolarization
Mitochondrial superoxide (MitoSOX)
ATP depletion
Calcium increase
Mem. Permeability (SYTOX/PI)
Membrane blebbing
LDH release
Addition of AG311
0
30
60
90
120
150
180
min